61 pages

THE STUDY OF MICROSTRIP ANTENNA ARRAYS AND RELATED PROBLEMS

1N - 28451

Semiannual Report

(20 May 1985 to 25 September 1986)

for

NASA NAG 3-418

National Aeronautics and Space Administration
Lewis Research Center
21000 Brookpark Road
Cleveland, OH 44135

NASA Technical Officer - R. Q. Lee

Prepared by

Y. T. Lo
Electromagnetics Laboratory
Department of Electrical and Computer Engineering
University of Illinois at Urbana-Champaign
1406 W. Green St.
Urbana, IL 61801

Technical Work

During this period efforts have been expended for the following tasks:

(1) Microstrip Antenna Module

In February, an initial computer program to be used in analyzing the four-element array module was completed. This program performs the analysis of modules composed of four rectangular patches which are corporately fed by a microstrip line network terminated in four identical load impedances. These identical load impedances are determined by ignoring mutual couplings which are believed to be second-order effects and by applying the cavity model theory to an individual, isolated patch. The resulting impedance at the module input is then determined by using transmission line theory and lumped, lossless circuits to represent the microstrip line corners and junctions.

Currently, a rigorous full-wave analysis of various types of microstrip line feed structures and patches is being carried out. As shown in Figure 1.0, these include the microstrip line feed and the electromagnetically coupled microstrip line feed between layers of different electrical parameters. The configuration for the array module remains unchanged except that the method of moments is now used to determine the input impedance. Mutual coupling is ignored at the moment, although it could be taken into account with more computational effort, and TEM transmission line theory is still used.

In the method of moments analysis, the distribution and magnitude of a primary electric or magnetic current source are assumed as the antenna excitation (e.g., electric current filament for coaxial probe feed or magnetic current ribbon for narrow feed gap), and the equivalence theorem is used to replace the antenna and feed lines by an unknown secondary current distribution. This secondary current distribution, which accounts for the scattering of the fields of the primary source by the antenna and feed structure, will in general contain two orthogonal components of current which flow in the plane of the antenna. Consequently, a vector dyadic Green's function must be used to obtain the fields of these individual components. By imposing the required boundary condition that the total tangential electric field on the surface of the antenna and the feed line is zero, a set of integral equations relating the components of the fields of the primary and secondary sources is obtained. The solution of the integral equations then yields an approximation to the vector components of the total current flowing on the structure. Unfortunately though, the solution of these currents requires the evaluation of integrals containing integrands which are oscillatory and very slowly decaying. But once these currents have been obtained, the input impedance may then be determined since the source excitation was assumed to be known.

At present, a method of moments program has been implemented for the case of a single dielectric layer and microstrip line fed

rectangular patches in which the primary source is assumed to be a magnetic current ribbon across the line some distance from the patch. It has been found that in order to obtain input impedance values which agree with measured values the location of this feed model on the feed line must approximately be at least one dielectric wavelength away from the patch edge.   Initial experiments have been conducted to examine this problem and determine at what distance from the patch along the microstrip line the fields are approximately TEM. Typical results are shown in Figure 2.0, where it is seen that impedance values can be translated by simple TEM transmission line theory wth reasonably good accuracy.   Further work on the theoretical modelling of the excitation is still required.

A typical example comparison of measured values with those computed by the program is shown in Figure 3.0. In this program, use has been made of subsectional "roof-top" basis functions as shown in Figure 4.0; therefore, the program has also been used to examine a few types of microstrip discontinuities as well.   A second program which analyzes multilayered dielectric structures of rectangular patches and electromagnetically coupled microstrip lines is nearly completed.   Like the first completed program, this version also uses subsectional basis and testing functions and is completely self-contained, needing no external libraries to perform complex matrix inversions, numerical integrations, or computation of special functions.

Both experimental and theoretical studies will continue concerning these feed structures. In particular, experimental work will be conducted to investigate theoretical primary source models other than the delta gap generator, the validity of the TEM transmission line model for different feed structures (such as co-planar waveguide), and the validity of the assumption of insignificant mutual coupling in alternate array modules. Amendments to the programs themselves are intended, such as the use of entire domain basis functions to improve computational efficiency.
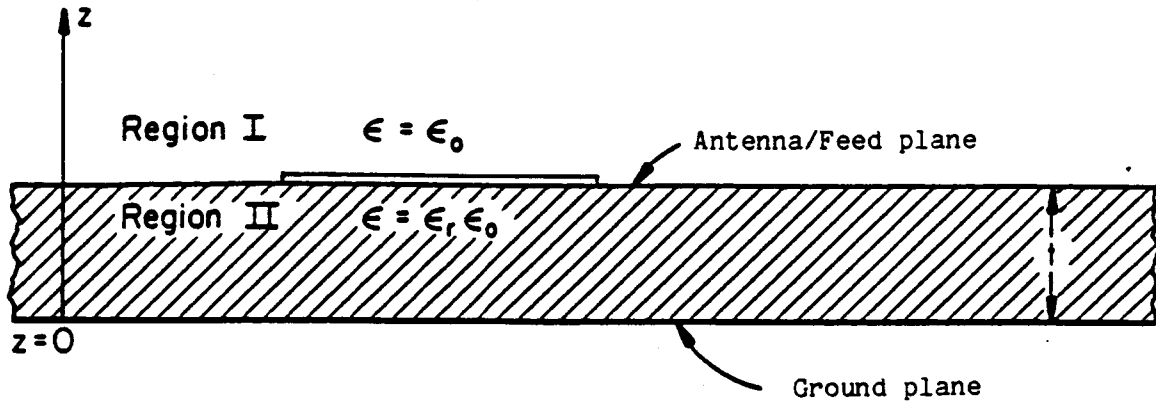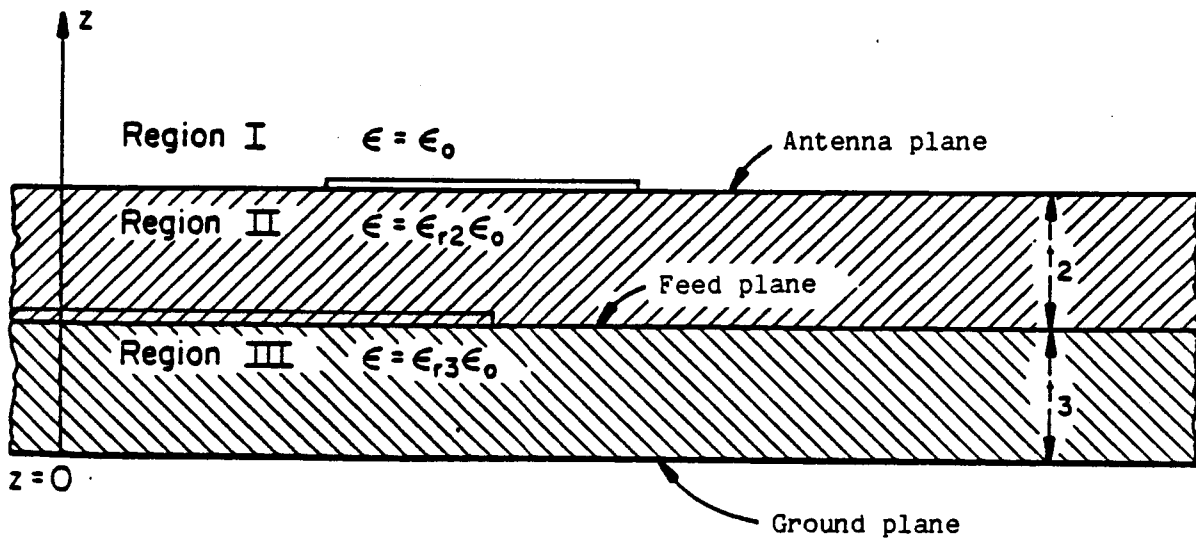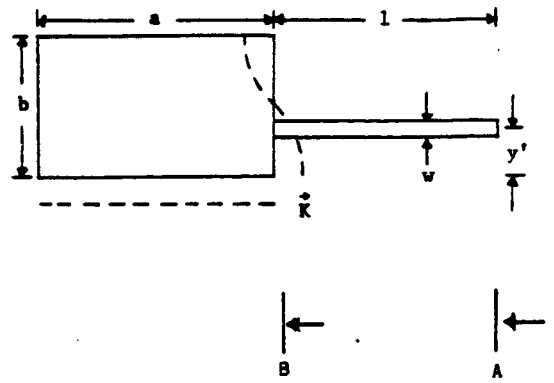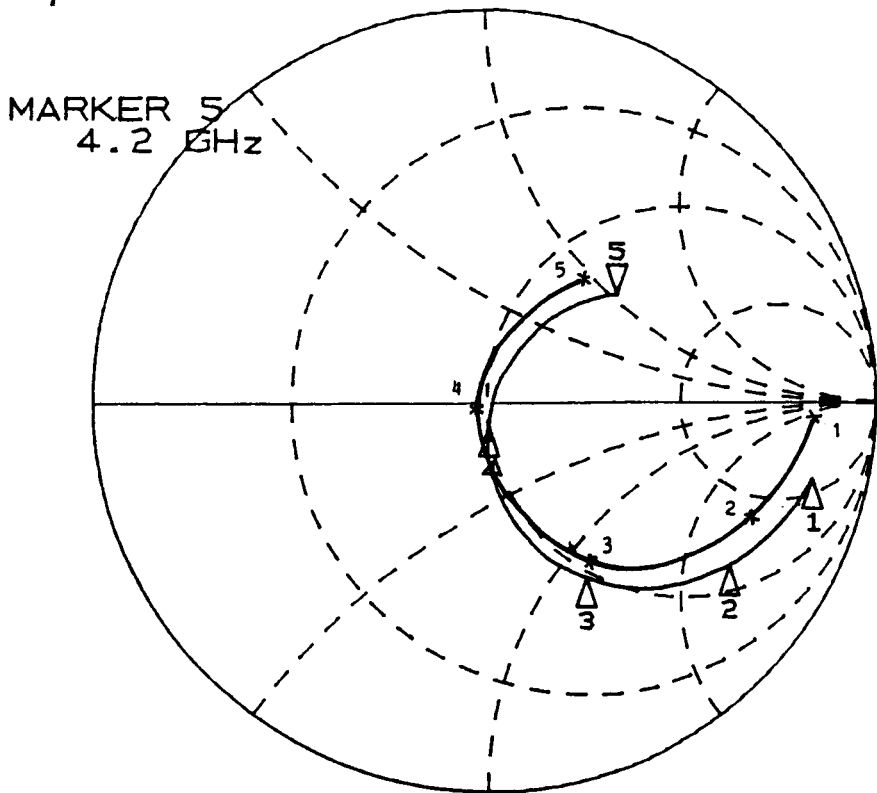
Figure 1.0 Physical structures of different feed networks being analyzed. (a) Patch and feed networks are constructed on a single dielectric slab. (b) Patch and feed networks are constructed on two dielectric layers having different electrical parameters.

MARKER 5
4.2 GHz

(a)

X = Measured at plane A, l= 2.7 cm (0.583 λ_ϵ @ 4.0 GHz)
△ = Measured at plane B, l=0.05 cm (0.01 λ_ϵ @ 4.0 GHz)
   a= 3.2 cm, b= 2.15 cm

Marker 1 = 3.8 GHz
Marker 2 = 3.9 GHz
Marker 3 = 4.0 GHz
Marker 4 = 4.1 GHz
Marker 5 = 4.2 GHz

MARKER 5
4.2 GHz
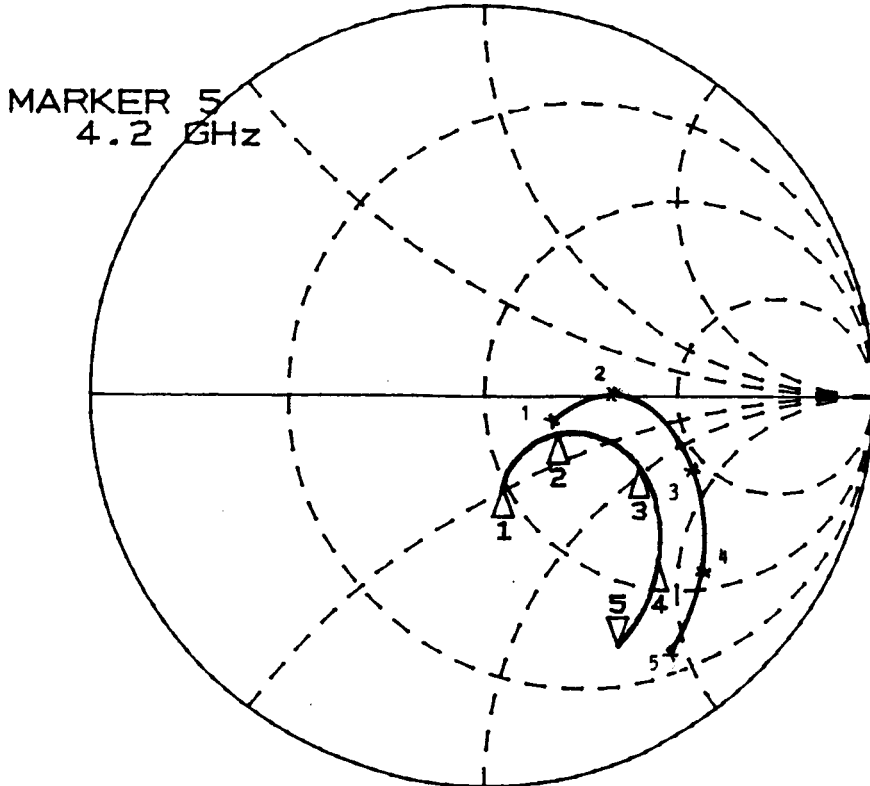
(b)

Figure 2.0   Comparison of input impedance loci measured at planes A and B
            where the values at plane A have been translated to plane B by
            simple TEM transmission line theory.   (a) Substrate is 0.034 λ_ϵ
            thick at 4.0 GHz. (b) Substrate is 0.069 λ_ϵ thick at 4.0 GHz.
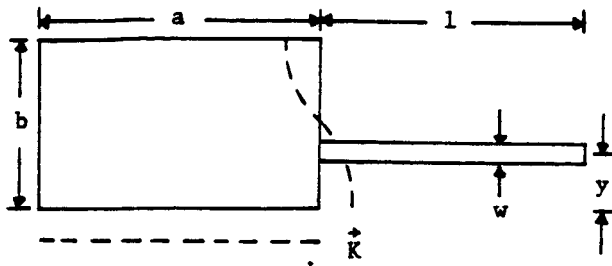
a= 3.2 cm b= 2.15 cm l= 2.7 cm $(0.583\lambda_\epsilon$ @ 4.0 GHz)

w= 0.44 cm y'= 0.4 cm   substrate thickness= 1/16" $(0.034\lambda_\epsilon$ @ 4.0 GHz)

ϵ_r = 2.62

MARKER 5
4.2 GHz

Marker 1 = 3.8 GHz
Marker 2 = 3.9 GHz
Marker 3 = 4.0 GHz
Marker 4 = 4.1 GHz
Marker 5 = 4.2 GHz

Experiment ———

Computed   X

START   3.800000000 GHz
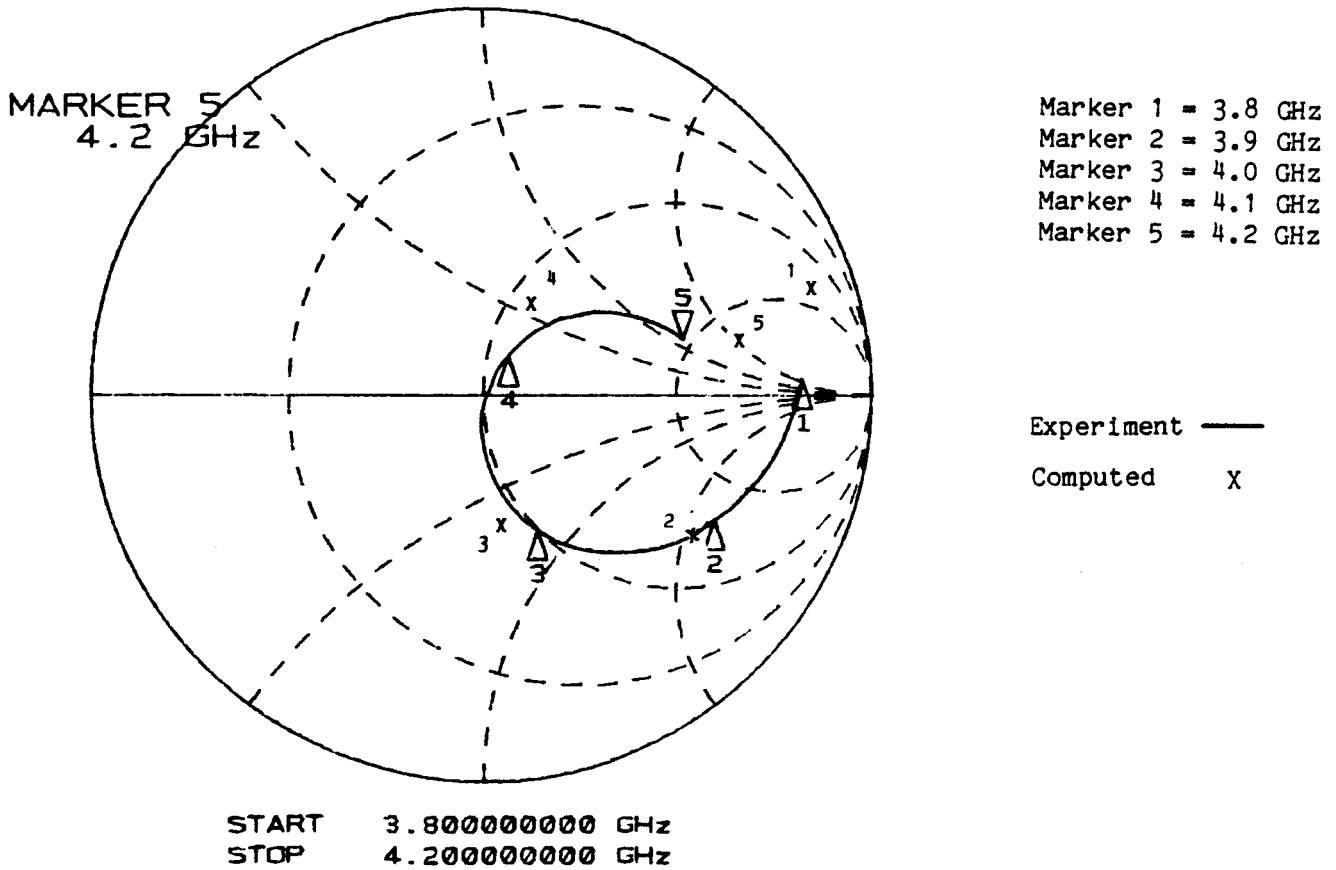STOP   4.200000000 GHz

Figure 3.0   Comparison of measured and computed input
impedance values for the case of a microstrip
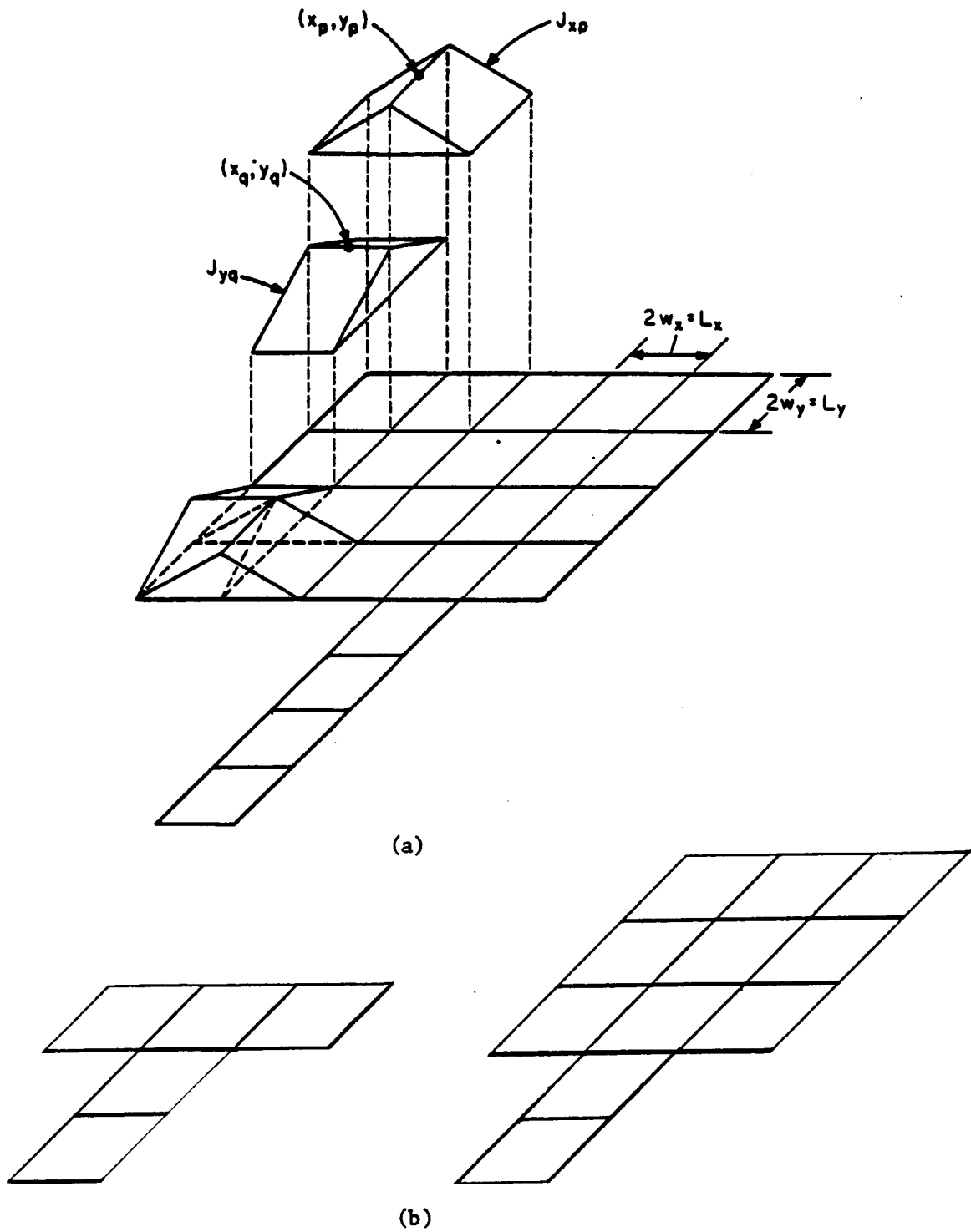fed patch.

(a)

(b)

Figure 4.0 (a) The basis function layout utilized in the method of moments
analysis. (b) The tee junction and step in width types of
microstrip line discontinuities which are analyzed through the
use of subsectional basis functions.

CHAPTER 1

INTRODUCTION

The first twenty years, following the introduction of the microstrip antenna in the early 1950's, were marked by few attempts to understand and analyze its characteristics. By the early 1970's, however, technological progress in the fields of integrated microwave electronics and mm-wave engineering had created the need for a new generation of antenna systems. The microstrip antenna, because of such unique properties as light weight, low profile, ease of manufacture, compatibility with integrated microwave components, etc., was seen as a promising candidate to satisfy the emerging requirements. This realization gave impetus to the tremendous expansion of microstrip antenna research and development witnessed in the past fifteen years. During this time virtually every engineering aspect of this antenna problem has been explored to some degree. Nevertheless, the major portion of the existing microstrip antenna literature is concerned with one specific topic, namely the input impedance problem. Interest in the input impedance problem is stimulated both by the designer's need for accurate characterization of the antenna's terminal properties, as well as by the theoretical challenge that the problem presents to the antenna engineer. The reason for this challenge becomes clear when it is recalled that precise calculation of the input impedance requires the solution of a formidable boundary value problem for the near fields of the antenna. Complicating the solution even further is the fact that the value of the input impedance is critically dependent upon the somewhat arbitrary choice of the antenna's input terminals. In fact [1] "to be able to define an antenna as a two-terminal element, it is necessary to define two electrically close points in the excitation region in which the feeder terminates and the antenna begins. This can be done fairly arbitrarily if rough analysis only is needed, but consider-

able care has to be exercised if more accurate analysis is required.

In spite of the assumed electrically small volume occupied by the excitation region, its geometry has considerable influence on the antenna impedance or admittance, although it practically does not influence the antenna radiation pattern. Therefore precise modeling of the antenna excitation region is necessary for obtaining accurate theoretical values of the antenna impedance or admittance."

From the preceding discussion it is clear that rigorous analytical formulation of the microstrip antenna problem alone is not sufficient to guarantee accurate input impedance results. Careful consideration of the excitation region appears to be just as important in input impedance calculations. Moreover, this aspect of the input impedance problem is far from trivial, leading certain investigators to conclude that [2] "the most difficult aspect of the patch radiator problem is the modeling of the feed. For one thing, many different types of feeds are possible: probe feeds, microstrip line feeds, proximity feeds, slot or aperture feeds, etc. Some of these feeds are very useful from a practical viewpoint, but are very difficult to treat analytically." There is little doubt that the feed modeling problem merits a great deal of attention. It will be the primary task of this thesis to study and model coaxial probe and microstrip transmission line feeds in the context of the overall microstrip antenna analysis.

The need for theoretical analysis of probe-fed microstrip antennas with electrically thick substrates is motivated by several major factors. Among these is the fact that microstrip antennas are currently being considered for use in millimeter-wave systems. The substrates proposed for such applications often have high relative dielectric constants and, hence, appear electrically thick. The necessity for greater bandwith is another major reason for studying thick substrate microstrip antennas. Consequently this problem, and

particularly the input impedance aspect of it, has received considerable attention in recent years. Several methods, varying in accuracy and computational effort requirements, have been proposed and used to calculate the input impedance and other parameters of probe fed microstrip antennas. The simpler of these methods is exemplified by the cavity model, in which the probe feed is replaced by a uniform current ribbon of equivalent width. The cavity model has been successfully used to calculate the input impedance of microstrip antennas with substrates ranging in thickness from 0.005 λ_ϵ to 0.02 λ_ϵ (λ_ϵ = wavelength in the dielectric) [3,4]. For thicker substrates, however, the cavity model, as well as other simpler models [22], have been abandoned in favor of the more rigorous moment method computations of the antenna patch currents. In references [5,6,21] moment method formulations were used to solve for currents on the rectangular patch fed by a current filament of 1 A. The effect of the probe was then simulated by adding a correction term to the calculated input impedance. In reference [7], a circular patch antenna fed by a uniform cylindrical current filament of finite radius was investigated. After removing the singular part of the current due to the feed, the patch currents were computed by using the vector Hankel transform and Galerkin's technique. Theoretical and experimental input impedance plots in [5-9] were compared for substrate thickness (t) ranging from 0.01 λ_ϵ to 0.035 λ_ϵ and no verification was given for t greater than 0.035 λ_ϵ. All of the formulations outlined above did not consider the actual feed structure in the analysis, replacing it instead by some idealized source.

An alternate approach to the problem of the probe fed circular microstrip antenna is presented in Chapter 2 of this thesis. As was already noted, a proper account of the metallic nature of the feed probe in the formulation could be very important, if not more, in the input impedance calculations. Therefore, instead of solving the open microstrip

structure problem using an idealized feed model as was done in [5-8], a solution satisfying the boundary conditions on the probe is obtained, utilizing the framework of the cavity model [3,4] so that the simplicity of using modal expansion in computation can be exploited. As in [4] all the losses, including the radiation, surface wave and copper losses are lumped into an effective loss tangent δ_{eff}. An edge extension formula [10] is used to account for the fringing of the fields at the edges of the patch. The analysis presented applies to the arbitrary location of the probe under the patch except for the uninteresting case of the probe very close to the edge.

In addition to the probe feed, a commonly employed method of exciting the printed patch antenna is by means of a microstrip transmission line. There exist several canonical feeding arrangements utilizing the microstrip line, namely the direct edge connection, capacitive edge feed, proximity feed, etc. Majority of past investigations of patch antennas fed by the microstrip transmission line were limited to the direct edge connection case [2,5,6,9]. Moreover, in many instances no distinction was made in the treatment of probe and microstrip line feeds, as the ideal current filament was used to model both types of feeds [2-4,6]. More realistic approaches to the problem of the proximity fed microstrip dipole were presented first by Oltman and Huebner [31], and recently in a more rigorous fashion by Katehi and Alexopoulos [27].

A method for computing the input impedance of a circular patch antenna excited by a microstrip transmission line is presented in Chapter 3. A distinguishing feature of the present analysis is the incorporation into the formulation of the boundary conditions on the feed. This kind of rigorous treatment has several advantages, namely it yields accurate input impedance results, and is applicable to a wide variety of feeding arrangements utilizing the microstrip transmission line. The problem is formulated in the Fourier

Transform domain. Moment method is applied to solve the integral equation for the currents on the patch and portion of the feed line. Considerable attention is given to acceleration of convergence of the Sommerfeld-type integrals which arise in the course of analysis.

The concluding chapter presents a summary and a discussion of the obtained results, pointing out the extent to which the original goals of this investigation were accomplished, and leading to suggestions for possible improvements and extensions of the present work.

CHAPTER 2

INPUT IMPEDANCE OF A PROBE FED

CIRCULAR MICROSTRIP ANTENNA WITH THICK SUBSTRATE

A method of computing the input impedance for the probe fed circular microstrip antenna with thick dielectric substrate is presented in this chapter. Utilizing the framework of the cavity model, the fields under the microstrip patch are expanded in a set of modes satisfying the boundary conditions on the eccentrically located probe, as well as on the cavity magnetic wall. A mode-matching technique is used to solve for the electric field at the junction between the cavity and the coaxial feed cable. The reflection coefficient of the TEM mode incident in the coaxial cable is determined, from which the input impedance of the antenna is computed. Measured data are presented to verify the theoretical calculations. Results of the computation of various losses as a function of substrate thickness for the circular printed antenna are also included.

In Section 2.I, a set of orthonormal modes for the circular waveguide with perfect magnetic (PMC) outer conductor and a perfect electric (PEC) inner conductor is constructed. The cutoff wavenumbers for this configuration are defined as the zeros of an infinite order determinant, whose elements are transcendental functions of the wavenumber. However, a truncated determinant can be used to compute the lowest cutoff frequencies with excellent precision [11,12]. The set of transverse modes, corresponding to the calculated cutoff wavenumbers, is found next. Each mode satisfies the boundary conditions on the outer (PMC) and inner (PEC) conductors. A procedure for normalizing the modes over the eccentric annular cross-section of the waveguide is outlined.

In Section 2.II a mode-matching technique is used to solve for the electric field in the annular aperture of the coaxial feed cable. The reflection coefficient of the TEM mode incident in the coaxial cable is determined, from which the input impedance of the antenna is computed.

Section 2.III contains a discussion of the results. Theoretical and experimental input impedance plots are compared for various values of substrate thicknesses, ranging from t = 0.03 λ_ϵ to t = 0.1 λ_ϵ. Finally, various losses for the circular microstrip patch versus its substrate thickness are presented.

2.I. Modes for the Eccentric Annular Waveguide

According to the cavity model, the circular microstrip antenna can be analyzed by assuming that the fields under the patch are essentially those of a magnetic wall cavity. The cavity is fed by a coaxial cable. The inner conductor of the cable spans the substrate and makes a contact with the patch. Figure 2.1(a) illustrates the resulting configuration. A transverse cross-section of the cavity, including the relevant coordinate systems, is shown in Fig. 2.1(b). The aim of this section is to construct a set of orthonormal modes for the waveguide having the eccentric annular cross-section of Fig. 2.1(b). The task can be simplified somewhat by making use of certain inherent symmetries. Since the TEM mode incident in the coaxial cable has no angular variation, it is expected that only even modes will be excited in the cavity. Moreover, it can be shown that the probe current excites predominantly the $\hat{z}$ component of electric field, and consequently the TM_z modes, in the cavity. TE_z modes will not be excited as strongly as the TM_z modes, and will be neglected henceforth.
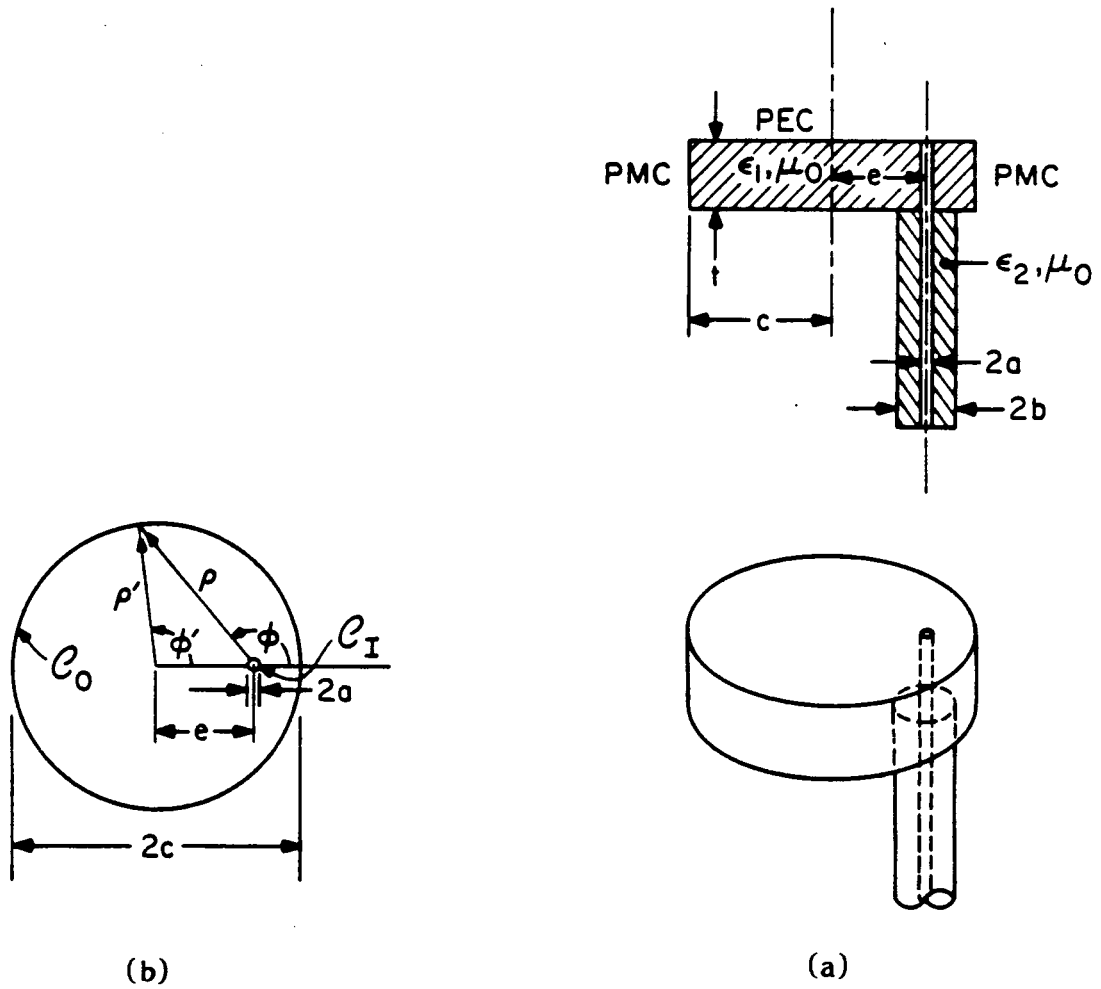
Figure 2.1.   Circular microstrip patch fed by a coaxial probe. (a) Cavity model of the patch. (b) Transverse cross-section of the magnetic wall cavity.

2.I.A. Cutoff wavenumbers and modes for the eccentric annular waveguide

Computation of cutoff frequencies and modes for eccentric annular domains, such as that in Fig. 2.1(b), has been the subject of several papers [11–13], on which the first part of this section is based. The transverse TM_z modal fields can be derived in the following manner [14]

$$e_q = -\frac{\nabla_t \psi_q}{k_q} \ , \ h_q = \hat{z} \times e_q \tag{2.1a}$$

$$(\nabla_t^2 + k_q^2)\psi_q = 0 \ , \ \text{B.C.:} \frac{\partial \psi_q}{\partial n} = 0 \ \text{on } C_O \ , \ \psi_q = 0 \ \text{on } C_I \tag{2.1b}$$

where a single-integer index set $\{q\}$ is used to enumerate the modes, and C_O, C_I denote the outer and inner conductor boundaries, respectively. A general solution of Helmholtz's Eq. (2.1b) in the (ρ, ϕ) coordinate system of Fig. 2.1(b) can be written as

$$\psi_q(\rho, \phi) = \sum_{m=0}^{\infty} C_{mq} B_m^{(m)}(k_q \rho) \cos(m\phi) \tag{2.2}$$

where $\{C_{mq}\}_{m=0}^{\infty}$ is a set of undetermined coefficients and $B_n^{(m)}(k_q \rho)$ is a combination of Bessel functions of first and second kind $J_n(\cdot)$ and $Y_n(\cdot)$, respectively. Although other combinations are possible, the particular one used here is given by

$$B_n^{(m)}(k_q \rho) = J_n(k_q \rho) - \frac{J_m(k_q a)}{Y_m(k_q a)} Y_n(k_q \rho) \tag{2.3}$$

Note that $B_m^{(m)}(k_q a) = 0$, which in turn implies that the boundary condition $\psi_q = 0$ on C_I is automatically accounted for by the expression in Eq. (2.2). However, the boundary condition on C_O still remains to be satisfied. This is accomplished by using the addition theorem for Bessel functions [15], to express ψ_q in the (ρ', ϕ') coordinate system as follows

$$\psi_q(\rho', \phi') = \sum_{m=0}^{\infty} C_{mq} \sum_{n=0}^{\infty} E(m,n,e) \, B_n^{(m)}(k_q\rho')\cos(n\phi') \, , \quad \rho' > e \tag{2.4}$$

where

$$E(m,n,e) = \frac{\gamma_n}{2} \left[J_{n-m}(k_q e) + (-1)^m \, J_{n+m}(k_q e) \right]; \qquad \gamma_n = \begin{cases} 1, & n=0 \\ 2, & n\neq 0 \end{cases}$$

and e is the distance separating the origins of the primed and the unprimed coordinate systems. Application of the boundary condition $\partial\psi_q/\partial\rho' = 0$ at $\rho' = c$ and use of orthogonality properties for trigonometric functions yield an infinite set of homogeneous equations with $\{C_{mq}\}_{m=0}^{\infty}$ as the unknowns. In order for this system of equations to have a nontrivial solution, its determinant must vanish. Denoting the determinant by $D_\infty(k_q)$ and its elements by $d_{nm}(k_q)$, the equation which the cutoff wavenumbers k_q must satisfy is given by

$$D_\infty(k_q) = 0 \tag{2.5a}$$

with

$$d_{nm}(k_q) = E(m,n,e) \, B'^{(m)}_n(k_q c), \quad m,n = 0,1,2... \tag{2.5b}$$

where the prime indicates differentiation with respect to the argument. A truncated, Mth order restriction of $D_\infty(k_q)$, denoted by $D_M(k_q)$, is used in the actual computation. The discussion of numerical techniques used in computing the k_q's is relegated to Section 2.III.

To complete the construction of the mode, the set of coefficients $\{C_{mq}\}_{m=0}^{M}$ must be found. From the numerical standpoint, this is a problem of solving a homogeneous system of equations with a vanishing determinant. Since the equations are dependent, C_{0q} can be set to equal one, and the resulting linear system solved for $\{C_{mq}\}_{m=1}^{M}$.

2.I.B. Normalization of modes in waveguides with eccentric annular cross-section

To be useful in subsequent calculations, the modes must be normalized over the cross-sectional area (S) of the guide. Mathematically, this is equivalent to finding a constant N_q, such that the following condition is satisfied

$$\int\int_S \hat{e}_q \cdot \hat{e}_q ds = 1 \tag{2.6}$$

where $\hat{e}_q$ is defined as $\hat{e}_q = \dfrac{e_q}{N_q}$.

Since the modes satisfy homogeneous boundary conditions on $C_0 + C_I$, Green's theorem can be used to derive the following expression for N_q:

$$N_q^2 = \int\int_S e_q \cdot e_q \, ds = \int\int_S \psi_q^2 \, ds \tag{2.7}$$

Evaluation of the integral in (2.7) can, of course, be performed by a straightforward substitution of expression (2.2) (or (2.4)) into (2.7). However, it is clear that such a substitution would result in a double summation of terms containing integrals of the following type

$$\int\int_S \left| B_m^{(m)}(k_q\rho) \, B_l^{(l)}(k_q\rho)\cos(m\phi)\cos(l\phi) \right| ds \tag{2.8}$$

Because of the complex nature of the eccentric annular domain of integration, a closed-form expression for Eq. (2.8) is not possible in general. Therefore, the straightforward approach to evaluation of Eq. (2.7) would suffer from computational inefficiency.

Fortunately, there exists an ingenious procedure for handling this problem. The detailed derivation can be found in [16] and will not be repeated here. The final result states

$$N_q^2 = \int\int_S \psi_q^2 \, ds = \oint_{C_I + C_O} \left| \frac{\partial \psi_q}{\partial(k_q^2)} \frac{\partial \psi_q}{\partial n} - \psi_q \frac{\partial^2 \psi_q}{\partial n \partial(k_q^2)} \right| dc \qquad (2.9)$$

This expression, after further simplification by using the boundary conditions in Eq. (2.1b), becomes

$$N_q^2 = \int\int_S \psi_q^2 \, ds = \oint_{C_O} (-\psi_q) \frac{\partial^2 \psi_q}{\partial n \partial(k_q^2)} \, dc + \oint_{C_I} \frac{\partial \psi_q}{\partial(k_q^2)} \frac{\partial \psi_q}{\partial n} \, dc \qquad (2.10a)$$

Close examination of Eq. (2.10a) reveals several important facts. First and foremost is the fact that evaluation of the contour integrals becomes trivial, when appropriate expressions for ψ_q are employed. This means that expressions (2.2) and (2.4) should be used on contours C_I and C_O, respectively. Moreover, it can be shown using expression (2.2) that the derivative of ψ_q with respect to k^2, evaluated at $k^2 = k_q^2$ and $\rho = a$, is identically zero. This implies that the contour integral on C_I must also vanish.

As noted in the previous paragraph, evaluation of the remaining contour integral on C_O is trivial. The result is in the form of a triple summation, which can be written as follows

$$N_q^2 = \frac{-\pi c^2}{2} \sum_{i=0}^{\infty} \sum_{j=0}^{\infty} C_{iq} \, C_{jq} \sum_{k=0}^{\infty} \frac{\gamma_k}{2} \left\{ (e/c) \left[J'_{k-i}(k_q e) + (-1)^i J'_{k+i}(k_q e) \right] B'^{(i)}_k(k_q c) + \right.$$

$$+ \left[J_{k-i}(k_q e) + (-1)^i J_{k+i}(k_q e) \right] \left[B''^{(i)}_k(k_q c) + \frac{2}{\pi k_q c} \frac{Y'_k(k_q c)}{Y_i^2(k_q a)} \right] \right\} \times$$

$$\times \left[J_{k-j}(k_q e) + (-1)^j J_{k+j}(k_q e) \right] B^{(j)}_k(k_q c) \qquad (2.10b)$$

where

$$B'^{(i)}_k(k_q c) = J'_k(k_q c) - \frac{J_i(k_q a)}{Y_i(k_q a)} Y'_k(k_q c)$$

$$B''^{(i)}_k(k_q c) = J''_k(k_q c) - \frac{J_i(k_q a)}{Y_i(k_q a)} Y''_k(k_q c)$$

and primes indicate differentiations with respect to argument. Numerical evaluation of the summations in Eq. (2.10b) is several orders of magnitude faster than the straightforward evaluation of Eq. (2.7) original proposed.

To recapitulate, a general derivation of modes for an eccentric annular waveguide was presented in this Section. A dispersion relation for the cutoff frequencies of such a waveguide was given, along with a method for finding the corresponding modes. Finally, a very efficient way of normalizing the modes over the cross-sectional domain of the guide was presented.

In the special case wherein the ratio of inner to outer conductor dimensions is small, perturbation techniques can be applied to derive analytical expressions for the cutoff wavenumbers and the corresponding modes. The procedure is illustrated in Appendix A, where annular cross-section waveguides with PEC and PMC outer boundaries of both circular and rectangular shape are considered.

2.II. Computation of Input Impedance

Consider the magnetic wall cavity fed by a coaxial cable, as illustrated in Fig. 2.1(a). It is assumed that a TEM mode is incident upon the annular aperture (A) formed by the junction between the coaxial cable and the cavity. In this section an integral equation for the tangential electric field $\mathbf{E}_a$ in the aperture, $A : a \leqslant \rho \leqslant b$, is derived. The integral equation is solved numerically by the mode-matching technique for the reflection coefficient (R) of the TEM mode, from which the input impedance for the circular

microstrip antenna is determined.

2.II.A. Derivation of the integral equation for the fields in the junction aperture A

The fields in the cavity region with permittivity ϵ_1 can be represented in terms of the set of orthonormal modes $\{\hat{e}_i\}_{i=1}^{\infty}$ derived in Section 2.I. At $z = 0^+$, the components of the field transverse to $\hat{z}$ can be expressed as

$$E_t(\rho, z=0^+) + \sum_{i=1}^{\infty} V_i \hat{e}_i(\rho) \qquad (2.11a)$$

$$-\hat{z} \times H_t(\rho, z=0^+) = \sum_{i=1}^{\infty} V_i Y_i \hat{e}_i(\rho) \qquad (2.11b)$$

where Y_i, $i=1,2,...$ are the modal admittances, at $z = 0^+$ given by

$$Y_i = -j \frac{\omega \epsilon_1}{k_{zi}} \cot(k_{zi}t) \;\; ; \;\; k_{zi} = \sqrt{\omega^2 \mu_o \epsilon_1 - k_i^2} \qquad (2.12)$$

Using the orthonormality property of the $\hat{e}_i$'s and Eq. (2.11a), the modal coefficients, V_i, can be expressed as follows

$$V_i = \iint_S E_t(\rho, z=0^+) \cdot \hat{e}_i(\rho) ds = \iint_A E_t(\rho, z=0^+) \cdot \hat{e}_i(\rho) ds \;\; ; \quad i=1,2,... \qquad (2.13)$$

where the domain of integration is reduced from S to A on account of the boundary condition which requires that $E_t(\rho, z=0^+)$ vanish on $S-A$.

The coaxial waveguide modes are well-known [17], and are briefly presented in Table 2.I for future reference. At $z=0^-$, the transverse fields in the coaxial cable can be represented in a complete set of orthonormal modes $\{\hat{e}'_j\}_{j=1}^{\infty}$ as follows

$$E_t(\rho, z=0^-) = (1+R)\hat{e}'_1(\rho) + \sum_{j=2}^{\infty} v_j \hat{e}'_j(\rho) \qquad (2.14a)$$

Table 2.I

MODES FOR THE COAXIAL WAVEGUIDE		
Type	Potential Function	$\hat{e}'$
TEM	$\chi_{00} = -\dfrac{ln(\rho)}{M_{00}}$	$\hat{e}_{00} = -\nabla_t \chi_{00}$
TM_z^{even}	$\chi_{\nu m} = \dfrac{F_m(\kappa_{\nu m}\rho)}{M_{1\alpha m}}\cos(m\phi)$, m=0,1,2...	$\hat{e}'_{\nu m} = \dfrac{-\nabla_t \chi_{\alpha m}}{\kappa_{\alpha m}}$
TE_z^{even}	$\chi_{\alpha n} = \dfrac{G_n(\kappa_{\alpha n}\rho)}{M_{2\alpha n}}\sin(n\phi)$, n=1,2,3...	$\hat{e}'_{\alpha n} = \dfrac{-\nabla_t \chi_{\alpha n}}{\kappa_{\alpha n}} \times \hat{z}$

$$F_m(\kappa_{\nu m}\rho) = J_m(\kappa_{\nu m}\rho)Y_m(\kappa_{\nu m}a) - J_m(\kappa_{\nu m}a)Y_m(\kappa_{\nu m}\rho)$$

$$G_n(\kappa_{\alpha n}\rho) = J_n(\kappa_{\alpha n}\rho)Y'_n(\kappa_{\alpha n}a) - J'_n(\kappa_{\alpha n}a)Y_n(\kappa_{\alpha n}\rho)$$

$$M_{00} = \left[2\pi\, ln(b/a) \right]^{1/2}$$

$$M_{1\nu m} = 2(\gamma_m \pi)^{-1/2}\kappa_{\nu m}^{-1}\left\{ \frac{J_m^2(\kappa_{\nu m}a)}{J_m^2(\kappa_{\nu m}b)} - 1 \right\}^{1/2}$$

$$M_{2\alpha n} = 2\pi^{-1/2}\kappa_{\alpha n}^{-1}\left\{ \left[\frac{J'_n(\kappa_{\alpha n}a)}{J'_n(\kappa_{\alpha n}b)}\right]^2 \left(1 - \frac{n^2}{(\kappa_{\alpha n}b)^2}\right) - \left(1 - \frac{n^2}{(\kappa_{\alpha n}a)^2}\right) \right\}^{1/2}$$

$$-\hat{z} \times H_t(\rho,z{=}0^-) = (1{-}R)y_1\hat{e}'_1(\rho) - \sum_{j=2}^{\infty} v_j y_j \hat{e}'_j(\rho) \qquad (2.14b)$$

where y_j's are the modal admittances given by

$$y_j = \sqrt{\epsilon_2/\mu_0} \ , \ \text{TEM mode } (j{=}1)$$

$$= \frac{\omega\epsilon_2}{\kappa_{zj}} \ , \ \text{TM}_z \text{ modes} \qquad (2.15)$$

$$= \frac{\kappa_{zj}}{\omega\mu_0} \ , \ \text{TE}_z \text{ modes}$$

and

$$\kappa_{zj} = \sqrt{\omega^2\mu_0\epsilon_2 - \kappa_j^2}.$$

The ϵ_2 is the medium permittivity in the coaxial waveguide and the κ_j's are the cutoff wavenumber of the coaxial waveguide, enumerated by the single-integer index set $\{j\}$. Again, since the infinite basis $\{\hat{e}'_j\}$ is orthonormal, it is possible to define modal coefficients v_j, $j{=}1,2,...$ as

$$v_j = \int\int E_t(\rho,z{=}0^-) \cdot \hat{e}'_j(\rho) ds \qquad (2.16)$$

where $v_1 = 1+R$.

Following the theory outlined in [19], expressions (2.11b) and (2.14b) are equated in order to satisfy the continuity conditions of the fields on A. Substitution of Eqs. (2.13) and (2.16) into the resulting equation and interchange of order of summation and integration [19] yield

$$2y_1\hat{e}'_1(\rho) = \int\int_A \left\{ \sum_{j=1}^{\infty} y_j \hat{e}'_j(\rho')\hat{e}'_j(\rho) + \sum_{i=1}^{\infty} Y_i \hat{e}_i(\rho')\hat{e}_i(\rho) \right\} \cdot E_a(\rho')d\rho' \qquad (2.17)$$

Equation (2.17) is the sought integral equation for the electric field E_a in the aperture A.

2.II.B. Solution of the integral equation by the mode-matching technique

The method for reducing the integral equation in (2.17) to a set of linear algebraic equations is well-known [19]. To briefly summarize, the field $E_a(\rho')$ is chosen to be approximated by a finite set of modes $\{\hat{e}'_n\}_{n=1}^{K}$, i.e.,

$$E_a(\rho') \simeq \sum_{n=1}^{K} v_n \hat{e}'_n(\rho') \qquad (2.18)$$

and the so-called intermodal coupling coefficient is defined in the following fashion:

$$I_{ij} = \iint_A \hat{e}_i \cdot \hat{e}'_j \, ds \qquad (2.19)$$

Computation of I_{ij} is in many instances facilitated by the use of Green's theorems and other vector calculus identities, in the manner demonstrated in Appendix B. The final expressions for the inner products between the coaxial cable modes, summarized in Table 2.I, and the cavity modes defined in Section 2.I are tabulated below.

Following [19], expression (2.18) is substituted into (2.17) and moments are taken with $\hat{e}'_m(\rho)$, $m=1,2,....,K$ to obtain a linear system of equations given by

$$[G]_{K \times K} [v]_{K \times 1} = [i]_{K \times 1}$$

$$G_{mn} = y_m \delta_{mn} + \sum_{i=1}^{L} Y_i I_{im} I_{in} \qquad (2.20)$$

$$i_m = 2y_1 \delta_{1m} \qquad \delta_{mn} = \begin{cases} 1 , & m=n \\ 0 , & m \neq n \end{cases}$$

The $K \times K$ matrix $[G]$ can be inverted to determine the modal coefficients v_j, $j=1,....,K$. The reflection coefficient R and the normalized input impedance Z_{in} are then determined by

Table 2.II

INNER PRODUCTS $I_{ij} = \int\int_A \hat{e}_i \cdot \hat{e}'_j \, ds$	
Mode types ⟍ cavity coax	$TM_z^{even} - \hat{e}_q$
$TEM - \hat{e}'_{00}$	$I_{(q)(00)} = \dfrac{-2\pi}{N_q M_{00} k_q} \, C_{0q} B_0^{(0)}(k_q b)$
$TM_z^{even} - \hat{e}'_{\nu m}$	$I_{(q)(\nu m)} = \dfrac{4}{\gamma_m} \dfrac{1}{N_q M_{1\nu m}} \dfrac{(k_q/\kappa_{\nu m})}{(\kappa_{\nu m}^2 - k_q^2)} \dfrac{J_m(\kappa_{\nu m} a)}{J_m(\kappa_{\nu m} b)} \, C_{mq} B_m^{(m)}(k_q b)$
$TE_z^{even} - \hat{e}'_{\alpha n}$	$I_{(q)(\alpha n)} = \dfrac{2n}{N_q M_{2\alpha n}} \dfrac{1}{k_q(\kappa_{\alpha n})^2 b} \, C_{nq} B_n^{(n)}(k_q b)$
	Note: Definitions of all the quantities appearing in this Table can be found in Table 2.I, Eqs. (2.2,2.3,2.10b), Figs. 2.1(a-b).

$$R = v_1 - 1 \text{ , and } Z_{in} = \frac{1+R}{1-R} \qquad (2.21)$$

The coefficients V_i can be calculated by using the following relation

$$V_i = \sum_{j=1}^{K} I_{ij} v_j \qquad i=1,2,....,L \qquad (2.22)$$

Once the V_i's are available, the total electric field in the cavity can be written as [14]

$$E_c(\rho,z) = \sum_{i=1}^{L} V_i(z)\hat{e}_i(\rho) + \frac{\hat{z}}{j\omega\epsilon_1} \sum_{i=1}^{L} I_i(z) \nabla_t \cdot \hat{e}_i(\rho) \qquad (2.23)$$

where

$$V_i(z) = V_i \frac{\sin[k_{zi}(t-z)]}{\sin(k_{zi}t)} \ , \quad I_i(z) = j\frac{\omega\epsilon_1}{k_{zi}^2} \frac{dV_i}{dz}$$

2.II.C. Discussion of the "effective dielectric loss" tangent calculation

Thus far, the microstrip antenna has been modeled by an ideal closed cavity. However, the antenna proper exhibits various loss mechanisms, including radiation and surface-wave excitation, and a method for incorporating these into the model must be found. One possible method is to lump the radiation, surface-wave, copper and dielectric losses into an "effective dielectric loss" tangent δ_{eff} and replace ϵ_1 in Eq. (2.12) by $\epsilon_1' = \epsilon_1(1-j\,\delta_{eff})$, as suggested in [4,18,20]. The quantity δ_{eff} is defined by the following expression

$$\delta_{eff} = \frac{P}{2\omega_r W_E} \tag{2.24}$$

where $P = P_{rad} + P_{sw} + P_{cu} + P_d$ is the total power lost due to radiation, surface-wave excitation, imperfectly conducting metallic portions of the cavity and in the dielectric. W_E is the time-averaged stored electric energy at the resonant frequency ω_r.

2.II.D. Evaluation of radiated and surface-wave power

Several methods exist for computing the radiated and surface wave power. The method used here assumes that a magnetic current $M = E_c \times \hat{n}\ |_{\rho'=c}$ is flowing on the outer PMC wall of the cavity, where $\hat{n}$ is the unit normal [3] outward from the cavity wall. The fields produced by M are found using the Fourier integral representation of the magnetic current Green's function for the grounded slab [14]. The surface-wave fields are found by evaluating the pole contributions of the Fourier representation integrals. The method of steepest descent is used to determine the space wave contribution of M.

As an example, consider the Green function for a transverse magnetic current source embedded in a PEC-backed dielectric slab of thickness t, and with constitutive parameters $\epsilon_1 = \epsilon_0 \epsilon_{r1}$, μ_o. The space- and surface-wave fields excited by the time-harmonic point source $\mathbf{M} = \hat{\tau}\, \delta(\rho-\rho')\delta(z-z')$, $\hat{\tau}$ being an arbitrary unit vector transverse to the $\hat{z}$ axis, and (ρ',z') denoting the source location, are given by the following set of expressions:

Radiated or space-wave fields

$$\left.\begin{aligned}
\mathbf{E}_{rad}(\mathbf{r},\mathbf{r}') &= \epsilon_{r1}j\mathbf{k}_o \times (j\mathbf{k}_o \times \hat{z})\, \Pi'_{rad}(\mathbf{r},\mathbf{r}') - j\omega\mu_o\, (j\mathbf{k}_o \times \hat{z})\Pi''_{rad}(\mathbf{r},\mathbf{r}') \\[2mm]
\mathbf{H}_{rad}(\mathbf{r},\mathbf{r}') &= j\omega\epsilon_1\, (j\mathbf{k}_o \times \hat{z})\, \Pi'_{rad}(\mathbf{r},\mathbf{r}') + j\mathbf{k}_o \times (j\mathbf{k}_o \times \hat{z})\, \Pi''_{rad}(\mathbf{r},\mathbf{r}')
\end{aligned}\right\} \qquad (2.25a)$$

$$\left.\begin{aligned}
j\omega\epsilon_1\, \Pi'_{rad}(\mathbf{r},\mathbf{r}') &= \hat{\tau} \times \hat{z} \cdot \nabla'_t\, G'_{rad}(\mathbf{r},\mathbf{r}') \\[2mm]
j\omega\mu_o\, \Pi''_{rad}(\mathbf{r},\mathbf{r}') &= \frac{1}{j\omega\mu_o}\, \hat{\tau}\, \frac{\partial}{\partial z'} \cdot \nabla'_t\, G''_{rad}(\mathbf{r},\mathbf{r}')
\end{aligned}\right\} \qquad (2.25b)$$

$$\left.\begin{aligned}
G'_{rad}(\mathbf{r},\mathbf{r}') &= \frac{2j\cot\theta}{k_o\sin\theta}\, Y'_{rad}(z,z')g_1(k_or)e^{jk_o\rho'\sin\theta\cos(\phi-\phi')} \\[2mm]
G''_{rad}(\mathbf{r},\mathbf{r}') &= \frac{2j\cot\theta}{k_o\sin\theta}\, Z''_{rad}(z,z')g_1(k_or)\, e^{jk_o\rho'\sin\theta\cos(\phi-\phi')}
\end{aligned}\right\} \qquad (2.25c)$$

where

$$Y'_{rad}(z,z') = \frac{\omega\epsilon_1\cos(k_{z1}z')e^{jk_{zo}t}}{[k_{zo}\epsilon_{r1}\cos(k_{z1}t) + jk_{z1}\sin(k_{z1}t)]}$$

$$Z''_{rad}(z,z') = \frac{j\omega\mu_o\sin(k_{z1}z')e^{jk_{zo}t}}{[k_{z1}\cos(k_{z1}t) + jk_{z1}\sin(k_{z1}t)]}$$

$$k_{zo} = k_o\cos\theta, \quad k_{z1} = k_o\sqrt{\epsilon_{r1}-\sin^2\theta}, \quad g_1(k_or) = \frac{e^{-jk_or}}{4\pi r}$$

∇'_t is the transverse "del" operator, applied to the source coordinates.

Surface-wave fields (TM$_z$ modes)

$$\left. \begin{array}{l} \mathbf{E}_{sw}(\mathbf{r},\mathbf{r}') = \dfrac{\epsilon_1}{\epsilon(z)} \; \nabla \times \nabla \times \hat{z} \; \Pi'_{sw}(\mathbf{r},\mathbf{r}') \\[2em] \mathbf{H}_{sw}(\mathbf{r},\mathbf{r}') = j\omega\epsilon_1 \; \nabla \times \hat{z} \; \Pi'_{sw}(\mathbf{r},\mathbf{r}') \\[2em] \epsilon(z) = \begin{cases} \epsilon_0, & t<z \\ \epsilon_1, & 0<z\leqslant t \end{cases} \end{array} \right\} \qquad (2.26a)$$

$$j\omega\epsilon_1 \; \Pi'_{sw}(\mathbf{r},\mathbf{r}') = \hat{r} \times \hat{z} \cdot \nabla'_t \, G'_{sw}(\mathbf{r},\mathbf{r}') \qquad (2.26b)$$

$$G'_{sw}(\mathbf{r},\mathbf{r}') = \dfrac{j}{2k_c} \; Y'_{sw}(z,z') g_2(k_c\rho) \, e^{jk_c\rho'\cos(\phi-\phi')} \qquad (2.26c)$$

where

$$Y'_{sw}(z,z') = \dfrac{j\omega\epsilon_1}{k_c D_E(\beta_0,\beta_1)} \times \begin{cases} \dfrac{\cos(\beta_1 z')\cos(\beta_1 z)}{\cos(\beta_1 t)}, & 0<z\leqslant t \\[1.5em] \cos(\beta_1 z')e^{-\beta_0(z-t)}, & t<z \end{cases}$$

$$D_E(\beta_0,\beta_1) = \sin(\beta_1 t)\left[\dfrac{k_0^2(\epsilon_{r1}-1)}{\beta_0^2\beta_1} + \dfrac{t(\beta_1^2 + \beta_0^2\epsilon_{r1}^2)}{\beta_0\beta_1\epsilon_{r1}} \right]$$

$$k_0 = \sqrt{k_c^2-k_0^2}, \; \beta_1 = \sqrt{k_0^2\epsilon_{r1}-k_c^2}; \; g_2(k_c\rho) = \sqrt{2/\pi k_c\rho} \; e^{-j(k_c\rho-\pi/4)}$$

dispersion relation for k_c : $(\beta_1 t) = (\beta_0 t)\epsilon_{r1}\cot(\beta_1 t)$

Surface wave fields (TE$_z$ modes)

$$E_{sw}(r,r') = -j\omega\mu_o \nabla \times \hat{z}\, \Pi''_{sw}(r,r')$$

$$H_{sw}(r,r') = \nabla \times \nabla \times \Pi''_{sw}(r,r')$$

$$\text{(2.27a)}$$

$$j\omega\mu_o\, \Pi''_{sw}(r,r') = \frac{1}{j\omega\mu_o}\, \hat{\tau}\frac{\partial}{\partial z'} \cdot \nabla'_t\, G''_{sw}(r,r') \qquad \text{(2.27b)}$$

$$G''_{sw}(r,r') = \frac{j}{2k_c}\, Z''_{sw}(z,z')\, g_r(k_c\rho)\, e^{k_c\rho'\cos(\phi-\phi')} \qquad \text{(2.27c)}$$

where

$$Z''_{sw}(z,z') = \frac{j\omega\mu_o}{k_c D_H(\beta_o,\beta_1)} \times \begin{cases} \dfrac{\sin(\beta_1 z')\sin(\beta_1 z)}{\sin(\beta_1 t)} & , \; 0<z\leqslant t \\[2mm] \sin(\beta z')\, e^{-j\beta_o(z-t)} & , \; t<z \end{cases}$$

$$D_H(\beta_o,\beta_1) = -\cos(\beta_1 t)\left\{ \left|\frac{(1+\beta_o t)(\beta_1^2+\beta_o^2)}{\beta_o^2\beta_1}\right| \right\}$$

dispersion relation for k_c : $(\beta_o t) = -(\beta_1 t)\cot(\beta_1 t)$

The power components P_{rad} and P_{sw} are calculated by integrating the corresponding Poynting vectors over the appropriate regions of space. Results of the numerical evaluation of various components of P for a specific antenna are presented in the following section.

2.III. Numerical and Experimental Results

Numerical results based upon previously performed theoretical analyses are presented in this section. Theoretical input impedance data are verified experimentally in all cases.

In Section 2.I a dispersion relation for the cutoff frequencies of a circular PMC waveguide with an eccentric inner PEC conductor was derived. The dispersion relation was given in the form of an infinitely dimensional characteristic determinant $D_\infty(k_q)$. The cutoff wavenumbers were defined as the zeros of this determinant. In actual computations, a truncated determinant of order M was used. Calculations of $\{k_q\}_{q=1}^{12}$ were performed for various ratios of a/c. It was found that the maximum discrepancy between the results for M=10 and M=15 is confined to within 1%. A graph of $\{k_q c\}_{q=1}^{5}$ is shown in Fig. 2.2. The ratio of inner to outer conductor radii for this particular case is a/c = 0.017. Note that as e goes to zero, the cutoff wavenumbers approach the well-known values of $k_q c$ for the concentric annular waveguide. In fact, these values can be utilized as initial estimates for the numerical root searching routines.

In Section 2.II a method of computing the input impedance Z_{in} for the circular microstrip antenna was presented. A mode-matching technique was used to solve for the reflection coefficient R of the TEM mode in the coaxial cable, from which Z_{in} was calculated. In all cases considered, the cavity radius c was much larger than the outer radius b of the coaxial cable. Consequently, the number of modes required to approximate E_a in the coaxial cable region was found to be considerably less than the corresponding number in the cavity region. Approximately eight to ten cavity modes were required to obtain numerical convergence. In contrast, only one or two coaxial cable modes were found to
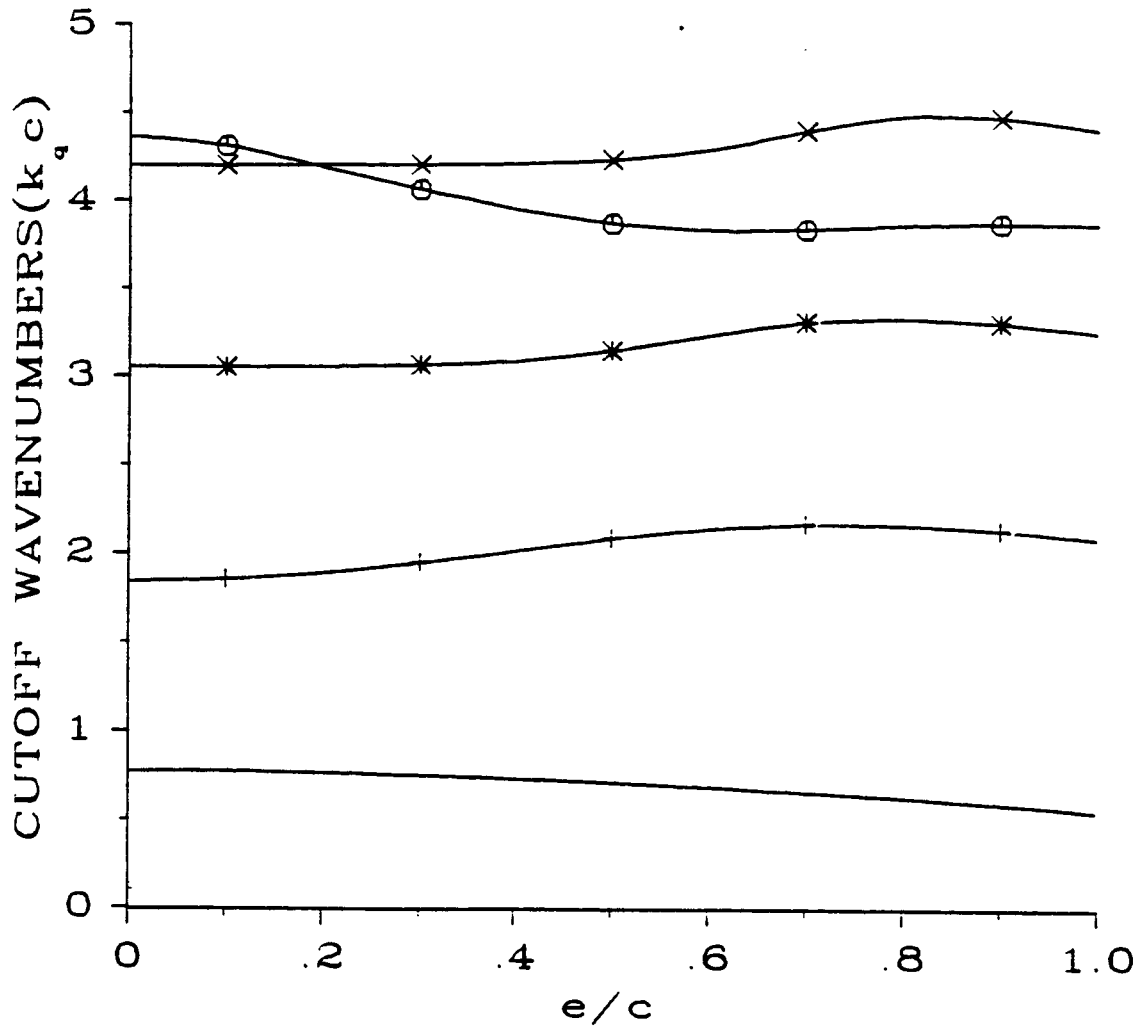
Figure 2.2.   Lowest five cutoff wavenumbers for a waveguide with a PMC outer conductor and an eccentrically located PEC inner conductor, a/c = 0.017.

give very accurate results, avoiding the need for inversion of large matrices. In fact, the problem could have been formulated from the outset by assuming a TEM field distribution in the aperture A and applying the variational method [18] to determine the input impedance.

In Figs. 2.3-2.5, Smith Chart plots of theoretically computed values of input impedance are compared with measurements for circular microstrip antennas of various sizes. The substrate material used in all cases was Rexolite 2200 with relative permittivity of 2.62 and a loss tangent of approximately 0.001. The input impedance loci were computed for two feed positions in each case. The curves numbered 1 and 2 in Figs. 2.3-2.5 correspond to feed locations of 7.5 mm and 10.5 mm, respectively, from the center of the patch. As noted previously, an edge extension formula [10] was used to account for the fringing field effect. As a result, the shift between the theoretical and experimental resonant frequencies is eliminated.

The results presented in Figs. 2.3-2.5 are for antennas with substrates ranging in thickness from 1.6 mm to 4.7 mm. In terms of the dielectric wavelength λ_ϵ, this is approximately equivalent to having t range from 0.03 λ_ϵ to 0.1 λ_ϵ. As the substrate thickness increases, analysis of input impedance data reveals several interesting trends. The expected shift of the impedance locus to the inductive side of the chart, as t increases, is clearly observed in Figs. 2.3-2.5. The shift is due to the fact that for large t the self-inductance of the probe constitutes a significant part of the overall antenna impedance. It is also observed that the bandwidth of the antenna markedly increases with substrate thickness. The bandwidths for SWR $<$ 3 and the Q factors for the three cases shown in Figs. 2.3-2.5 are given in Table 2.III, along with the relevant antenna dimensions.
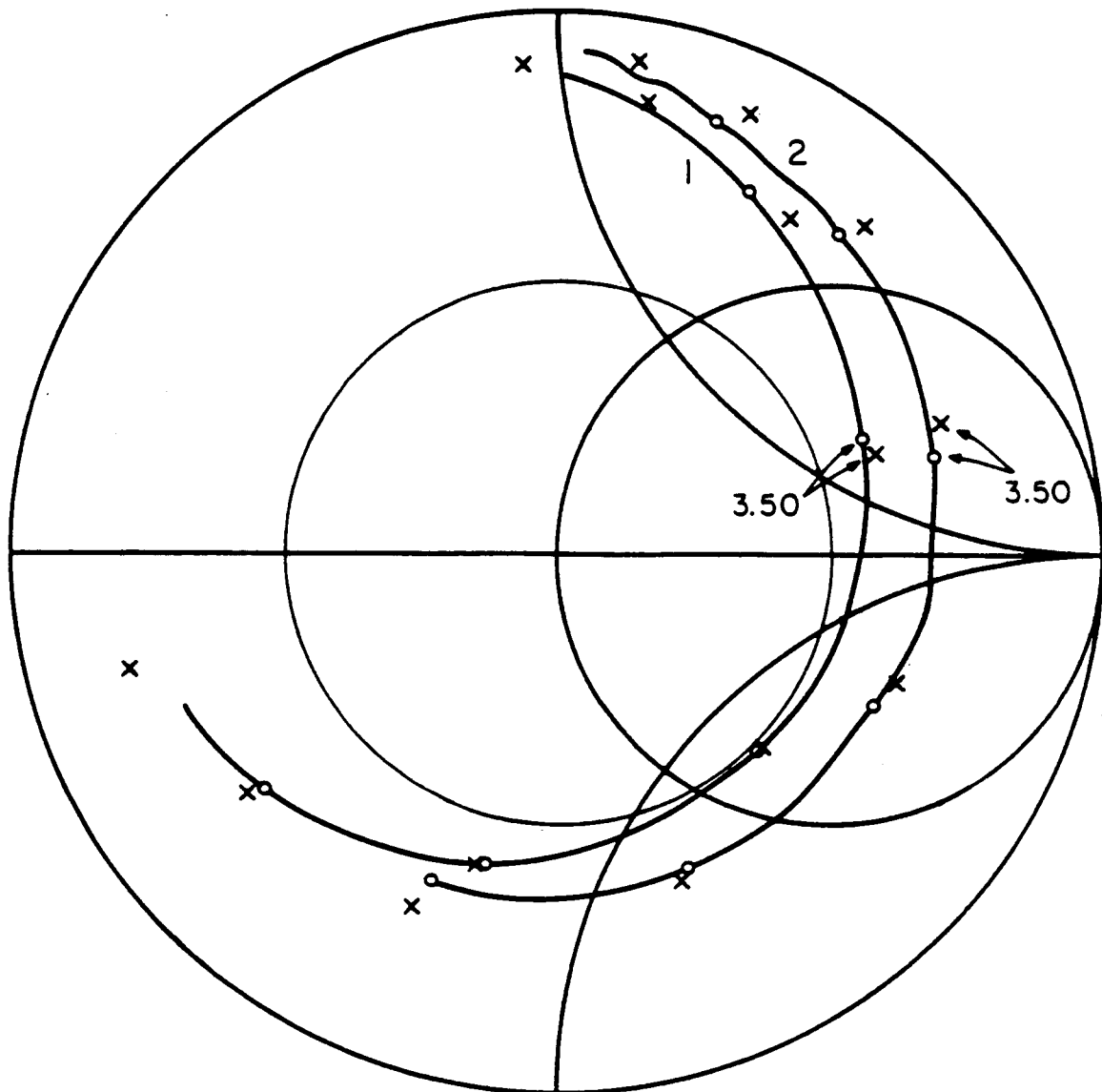
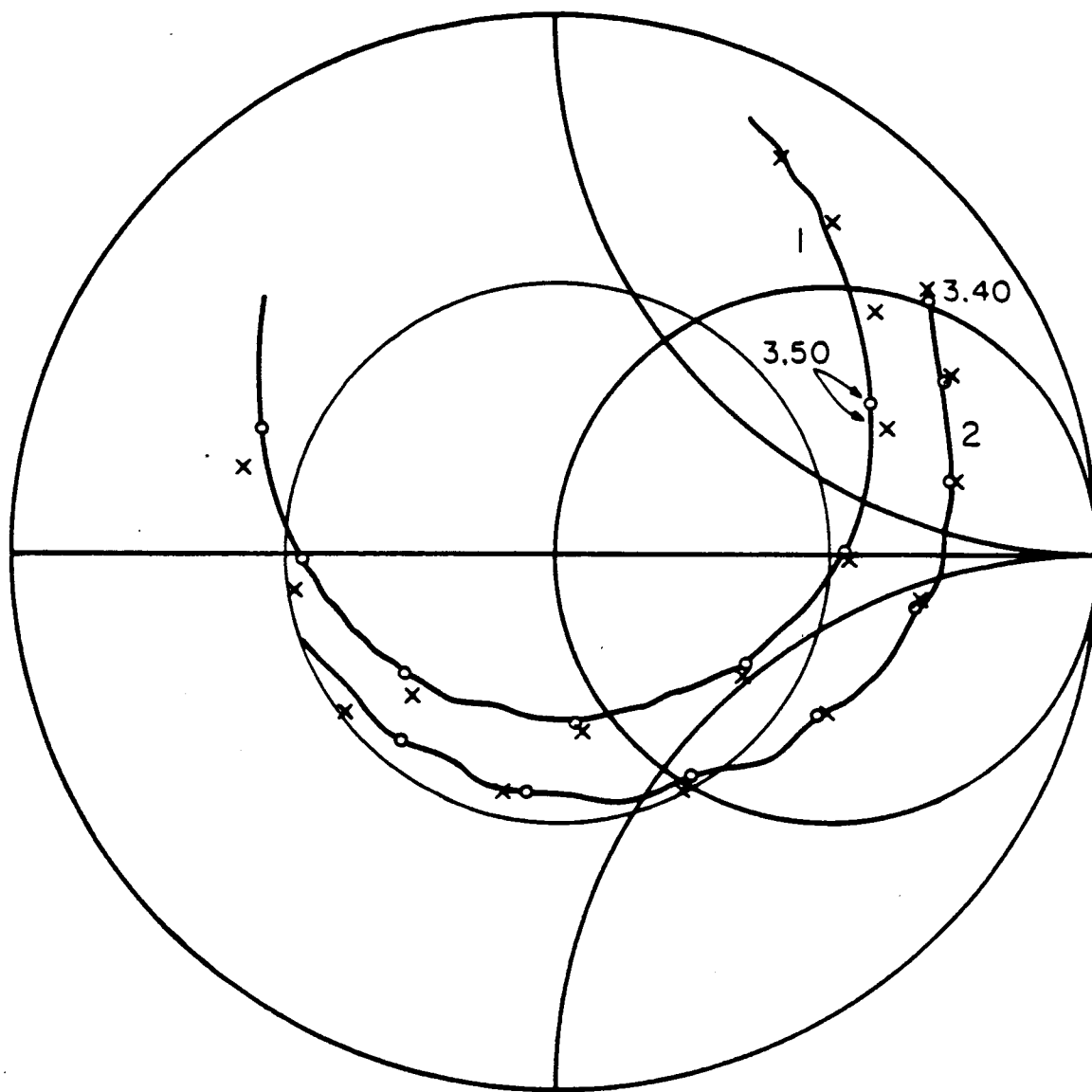Figure 2.3.   Measured and computed impedance loci: c = 14.1 mm, t = 1.6 mm, e_1 = 7.5 mm, e_2 = 10.5 mm, ϵ_1 = 2.62.

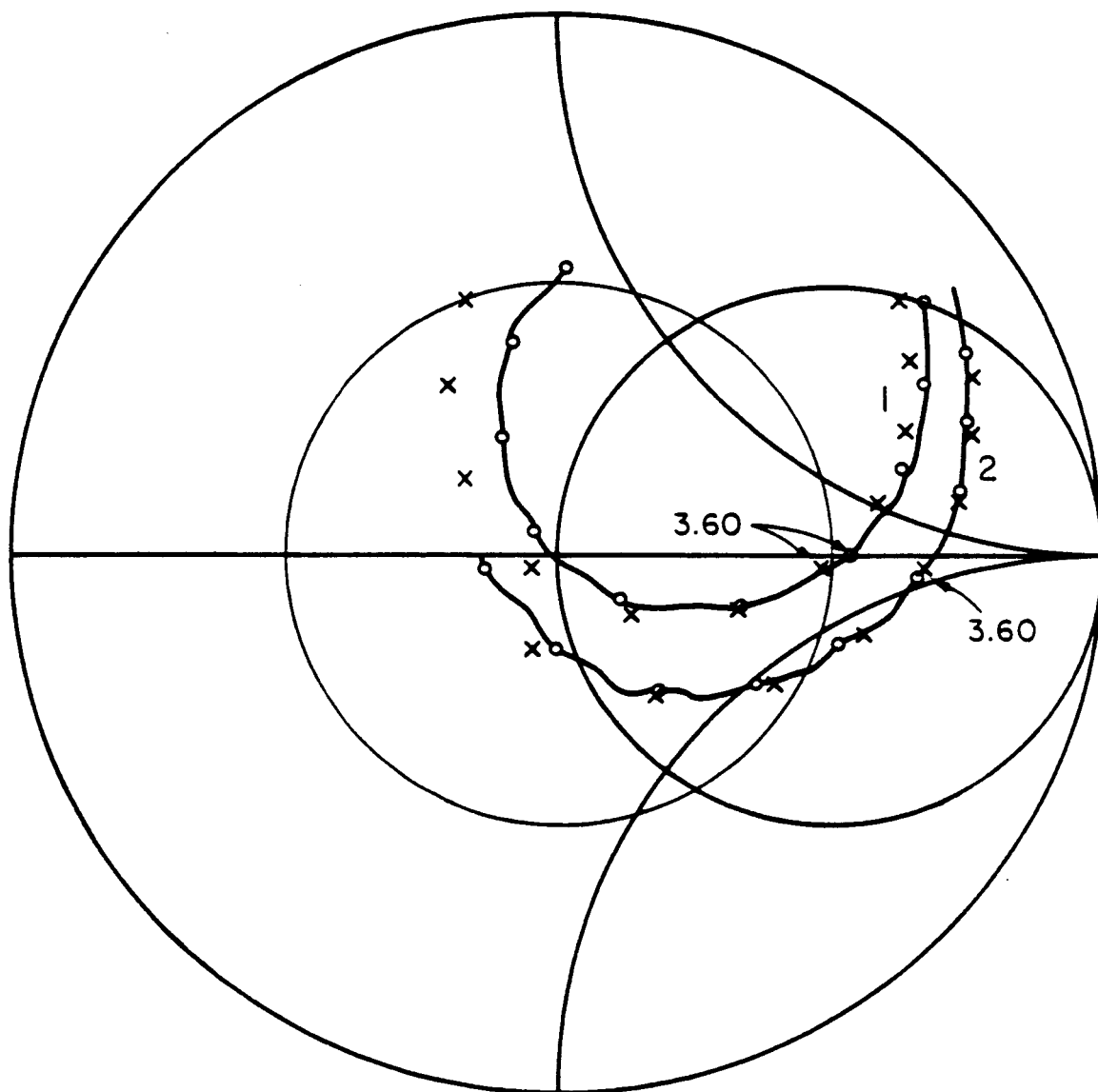Figure 2.4.   Measured and computed impedance loci: c = 13.5 mm, t = 3.2 mm, e_1 = 7.6 mm, e_2 = 10.5 mm, ϵ_1 = 2.62.

Figure 2.5. Measured and computed impedance loci: c = 13.0 mm, t = 4.7 mm, e_1 = 7.5 mm, e_2 = 10.5 mm, ϵ_1 = 2.62.

Table 2.III

Estimated Bandwidths and Q Factors

Antenna dimensions	Q factor	Bandwidth (VSWR < 3:1)
c = 14.1 mm t = 1.6 mm	33	5%
c = 13.5 mm t = 3.18 mm	15	10%
c = 13.0 mm t = 4.8 mm	9	18%

Finally, Fig. 2.6 depicts proportions of various power losses for the circular printed antenna of radius 0.25 λ_ϵ as a function of substrate thickness. It is seen that while the dielectric and copper losses become relatively insignificant the surface wave power increases with thickness and as much as 30% of the power can be lost through surface-wave excitation. As a result, the radiation efficiency of the antenna can fall below an acceptable level. Thus, it appears that for broadside radiation, very thick microstrip antennas, although having broad-band impedance characteristics, may not be desirable from the radiation efficiency point of view.
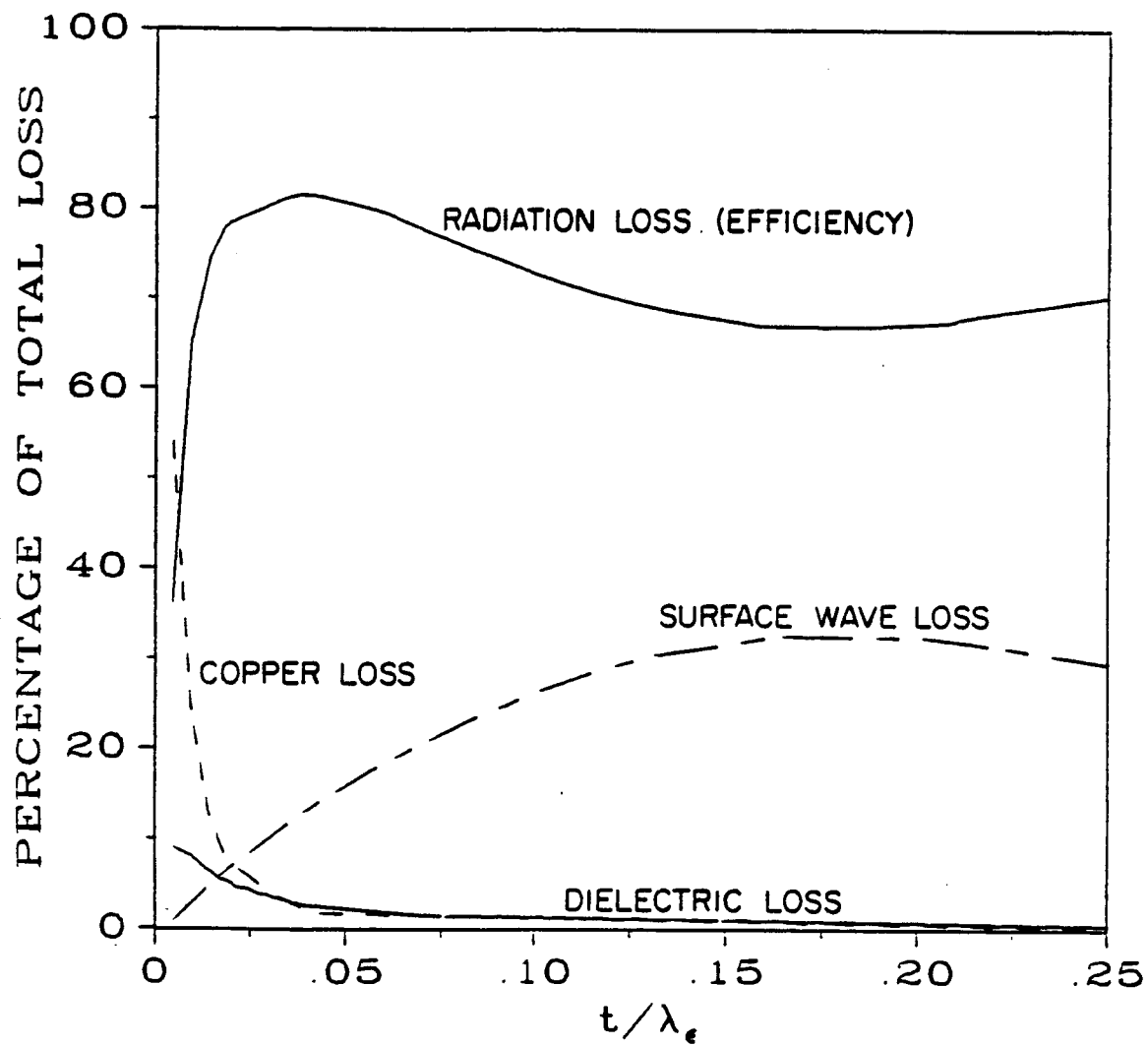
Figure 2.6.   Computed losses for the circular printed antenna of radius 0.25 λ_ϵ.

LIST OF REFERENCES

[1]   B.D. Popovic', M.B. Dragovic', and A.R. Djordjevic', *Analysis and Synthesis of Wire Antennas*, England: Research Studies Press, 1982.

[2]   D.M. Pozar and D.H. Schaubert, "Analysis of infinite array of rectangular microstrip patches with idealized probe feeds," *IEEE Trans. Antenna Propagat.*, vol. Ap-32, no. 10, pp. 1101 W. Springfield Ave.-1107, Oct. 1984.

[3]   Y.T. Lo, D. Solomon, and W.F. Richards, "Theory and experiment on microstrip antennas," *IEEE Trans. Antennas Prpagat.*, vol. AP-27, no. 2, pp. 137-145, Mar. 1979.

[4]   W.F. Richards, Y.T. Lo, and D.D. Harrison, "An improved theory for microstrip antennas and applications," *IEEE Trans. Antennas Propagat.*, vol. AP-29, no. 1, pp. 38-46, Jan. 1981.

[5]   E.H. Newman and P. Tulyathan, "Analysis of microstrip antennas using moment method," *IEEE Trans. Antennas Propagat.*, vol. AP-29, no. 1, pp. 47-53, Jan. 1981.

[6]   D.M. Pozar, "Input impedance and mutual coupling of rectangular microstrip antennas," *IEEE Trans. Antennas and Propagat.*, vol. AP-30, pp. 1191-1196, Nov. 1982.

[7]   W.C. Chew and J.A. Kong, "Analysis of a circular microstrip disk antenna with a thick dielectric substrate," *IEEE Trans. Antennas Propagat.*, vol. AP-29, no. 1, pp. 68-76, Jan. 1981.

[8]   S. Yano and A. Ishimaru, "A theoretical study of the input impedance of a circular microstrip disk antenna," *IEEE Trans. Antennas Propagat.*, vol. AP-29, no. 1, pp. 77-84, Jan. 1981.

[9]   M.D. Deshpande and M.C. Bailey, "Input impedance of microstrip antennas," *IEEE Trans. Antennas Propagat.*, vol. AP-30, no. 4, pp. 645-650, July 1982.

[10]   L.C. Shen, S.A. Long, M.R. Allerding, and M.D. Walton, "Resonant frequency of a circular disc printed circuit antenna," *IEEE Trans. Antennas Propagat.*, vol. AP-25, no. 4, pp. 595-596, July 1977.

[11]   G.I. Veselov and S.G. Semenov, "Theory of circular waveguide with eccentrically placed metallic conductor," *Radio Eng. Electron. Phys.*, vol. 15, no. 4, pp. 687-690, 1970.

31 - 55

[12]   K. Nagaya, "Vibration of a membrane having a circular outer boundary and an eccentric circular inner boundary," *J. Sound Vibration*, vol. 50, pp. 545-551, 1977.

[13]   James R. Kuttler, "A new method for calculating TE and TM cutoff frequencies of uniform waveguides with lunar or eccentric annular cross section," *IEEE Trans. Microwave Theory Tech.*, vol. 32, no. 4, pp. 348-354, Apr. 1984.

[14]   L.B. Felsen and N. Marcuvitz, *Radiation and Scattering of Waves*, New Jersey: Prentice Hall, 1973.

[15]   M. Abramowitz and I. Stegun, *Handbook of Mathematical Functions*. New York: Dover, 1972.

[16]   P.M. Morse and H. Feshbach, *Methods of Theoretical Physics*. *New York: McGraw-Hill, 1953*.

[17]   N. Marcuvitz, ed., *Waveguide Handbook*, Radiation Laboratory Series, vol. 10. New York: McGraw-Hill, 1951.

[18]   R.F. Harrington, *Time-Harmonic Electromagnetic Waves*. New York: McGraw-Hill, 1961.

[19]   N. Amitay, V. Galindo, and C.P. Wu, *Theory and Analysis of Phased Array Atennas. New York: Wiley-Interscience*, 1972.

[20]   W.F. Richards, et al., "Theory and Applications for Microstrip Antennas," in Proc. Workshop on Printed Antenna Tech., New Mexico State Univ., Las Cruces, oct. 1979, pp. 8/1-20.

[21]   S.M. Wright, "Efficient Analysis of Infintie Microstrip Arrays on Electrically Thick Substrates," Ph.D. dissertation, Dept. Elec. Eng., University of Illinois, Champaign, Urbana, 1984.

[22]   D.L. Sengupta, "Transmission line analysis of rectangular patch antennas," *Electromagnetics*, vol. 4, pp. 355-376, Dec. 1984.

[23]   W.H. Eggimann, "Higher order evaluation of electromagnetic diffraction by circular discs," *IEEE Trans. Microwave Theor. Tech.*, vol. 9, no. 5, pp. 408-418, Sept. 1961.

[24]   J.J. Bowman, T.B.A. Senior, P.L.E. Uslenghi, ed., *Electromagnetic and Acoustic Scattering by Simple Shapes*. Amsterdam: North-Holland Publishing Co., 1969.

[25]   W.F. Richards, "Anisotropy, Birefringence and Dispersion in Artificial Dielectrics," Ph.D. dissertation, Dept. Electrical Engineering, University of Illinois at Urbana-Champaign, 1977.

[26]   I.S. Gradshteyn, I.M. Ryzhik, *Table of Integrals, Series, and Products.* Florida: Academic Press, 1980.

[27]   P.B. Katehi, N.G. Alexopoulos, "On the modeling of electromagnetically coupled microstrip antennas - the printed strip dipole," IEEE Trans. Antennas Propagat., vol. 32, no. 11, pp. 1179-1186, November 1984.

[28]   R.W. Jackson, D.M Pozar, "Full wave analysis of microstrip open-end and gap discontinuities," *IEEE Trans. Microwave Theory Tech.*, vol. 33, no. 10, pp. 1036-1043, October 1985.

[29]   P.B. Katehi, N.G. Alexopoulos, "Frequency dependent characteristics of microstrip discontinuities in millimeter-wave integrated circuits," *IEEE Trans. Microwave Theory Tech.*, vol. 33, no. 10, p. 1029-1036, October 1985.

[30]   J.R. James, P.S. Hall, C. Wood, *Microstrip Antennas: Theory and Design.* London: Peregrinus, 1981.

[31]   H.G. Oltman, D.A. Huebner, "Electromagnetically coupled microstrip dipoles," *IEEE Trans. Antennas Propagat.*, vol. 29, pp. 151-157, Jan. 1981.

[32]   R.S. Elliott, G.J. Stern, "The design of microstrip dipole arrays including mutual coupling, Part I: Theory," *IEEE Trans. Antennas Propagat.*, vol. 29, no. 5, pp. 757-760, Sept. 1981.

[33]   G.J. Stern, R.S. Elliott, "The design of microstrip dipole arrays including mutual coupling, Part II: Experiment," *IEEE Trans. Antennas Propagat.*, vol. 29, no. 5, pp. 761-765, Sept. 1981.

[34]   W. Gautschi, "Computational aspects of three-term recurrence relations," SIAM Review, vol. 9, no. 1, January, 1967.

[35]   F.E. Eastep, "Estimation of fundamental frequency of doubly-connected membranes," *J. Sound Vibration*, vol. 37, no. 3, pp. 399-410, 1974.

[36]   M. Davidovitz and Y.T. Lo, "Input impedance of a probe-fed circular microstrip antenna with thick substrate," *IEEE Trans. Antennas Prop.* vol. 34, no. 7, pp. 905-911, July 1986.

[37]   R.E. Collin, *Field Theory of Guided Waves*. New York: McGraw-Hill Book Co., 1960.

APPENDIX A

CUTOFF WAVENUMBERS AND MODES FOR ANNULAR CROSS-SECTION WAVEGUIDE WITH ECCENTRIC INNER CONDUCTOR OF SMALL RADIUS

A.I. Introduction

Computation of cutoff wavenumbers for uniform waveguides with eccentric annular cross-section has been the subject of numerous investigations [11-13,35].[1] Various techniques suggested for that purpose are for the most part rigorous in nature, and require considerable numerical analysis. A relatively important limiting case which has not received much attention, and yet is of practical interest, is the annular waveguide with small ratio of inner to outer conductor dimensions. Configurations of this type arise, for example in the analysis of cavities excited by thin probes [36].

The purpose of this appendix is to derive approximate analytical expressions for the cutoff wavenumbers and the corresponding modal wavefunctions for annular waveguides with small ratios of inner to outer conductor dimensions. Derivation of the results is based to a large extent on the perturbation technique outlined in the investigation entitled "Distortion of Standing Wave by a Strip," found in reference [16].

Circular waveguide with eccentrically located inner conductor of small radius is analyzed in Section A.II. Cutoff wavenumbers computed therein are compared with data numerically generated from a more rigorous formulation [11].

Section A.III considers the case of rectangular waveguide with arbitrarily located small inner conductor. Again, the cutoff wavenumbers and the corresponding modal wavefunctions are derived.

---

1   Only a partial list of relevant publications is referenced.

A.II. Circular Waveguide with an Eccentric Inner Conductor of all Radius

Approximate formulas for the cutoff wavenumbers and the corresponding modes in a circular waveguide with eccentric inner conductor of small radius are derived in this section. A cross-section of the waveguide, with the relevant dimensions indicated, is shown in Figure A1. Analysis of the TM modes is presented in detail. The results for the TE case can be obtained in an analogous manner.

The TM modes in a uniform waveguide can be derived from a scalar potential function $\psi_{\nu m}$ satisfying the wave equation

$$(\nabla_t^2 + k_{\nu m}^2)\psi_{\nu m} = 0 \ , \tag{A1}$$

and subject to appropriate boundary conditions [14]. In the absence of the inner conductor in a circular waveguide having a PEC outer boundary of radius c, the solution of Eq. (A1) is known to be

$$\psi_{\nu m} = J_m(k_{\nu m}\rho')\cos(m\phi') \quad ; \quad J_m(k_{\nu m}c) = 0 \tag{A2}$$

where J_m denotes a Bessel function of the first kind of order m. It is intuitively clear that the presence of a small inner conductor slightly perturbs the above solution. Derivation of the modified solution, denoted by $\Psi_{\nu m}$, is facilitated by the introduction of several hypotheses, detailed discussion of which can be found in [16]. A brief restatement thereof follows.

Initially it is assumed that the standing wave $\psi_{\nu m}$, which is expressible as a combination of diverging and converging cylindrical waves, is incident upon the inner conductor and is scattered by it. The effect of the scatterer on the incident waves is computed as though these waves were out in the unbounded medium, i.e. with the outer wall boundary C_0 at infinity. It is hypothesized that the value of $\Psi_{\nu m}$ at the inner conductor
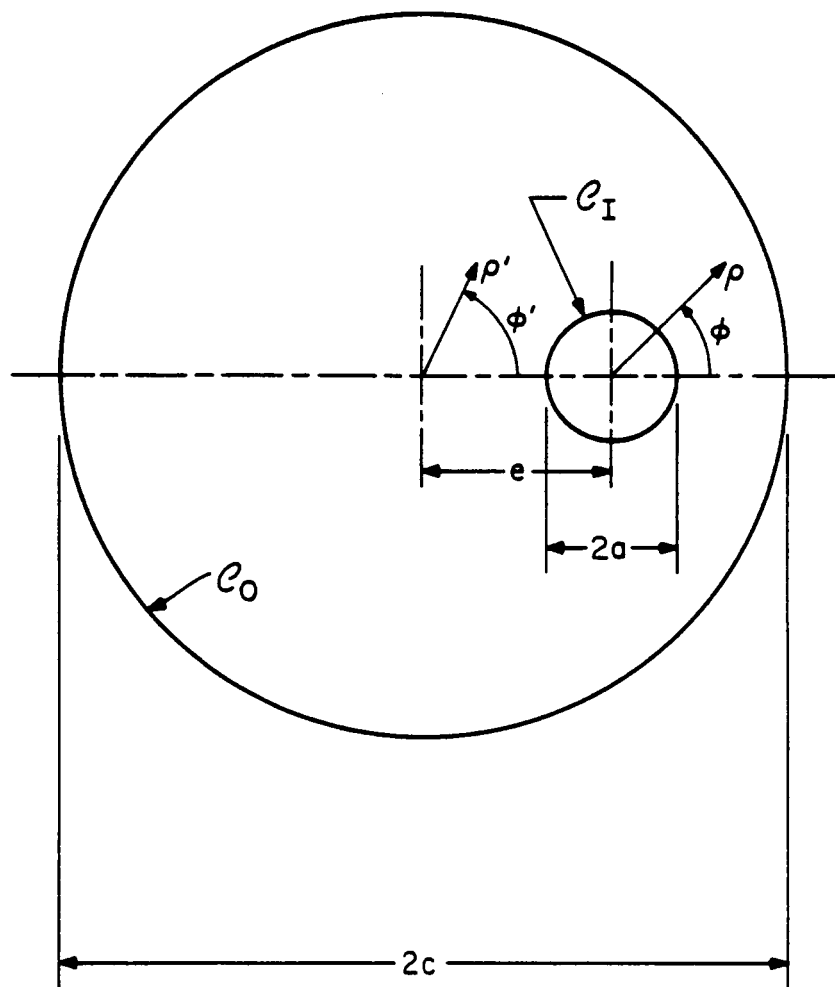
Figure A1.   Cross-section of an annular waveguide with circular outer conductor.

boundary C_I should not be very sensitive to the presence or absence of the outer wall, so long as the inner conductor is small and is not situated close to C_O. Consequently, the behavior of $\Psi_{\nu m}$ on C_I is known fairly accurately from the analysis performed with C_O at infinity. The behavior of the modified wavefunction $\Psi_{\nu m}$ in the rest of the waveguide cross-section can be found with the aid of the following equation

$$\Psi_{\nu m}(\rho_o^{'},\phi_o^{'}) = -\oint_{C_I} \frac{\partial \Psi_{\nu m}}{\partial n}(\rho_s^{'},\phi_s^{'})\, G(\rho_o^{'},\phi_o^{'}|\rho_s^{'},\phi_s^{'})dc \quad , \tag{A3}$$

derived using Green's theorem. The subscripts "o" and "s" in the above equation refer to the observation and source coordinates, respectively. $G(\rho_o^{'},\phi_o^{'}|\rho_s^{'},\phi_s^{'})$ denotes the scalar Green function satisfying the appropriate boundary condition on C_O. In the case of a PEC outer boundary, application of standard analytical techniques yields the following expression for $G(\rho_o^{'},\phi_o^{'}|\rho_s^{'},\phi_s^{'})$

$$G(\rho_o^{'},\phi_o^{'}|\rho_s^{'},\phi_s^{'}) = \sum_{n=0}^{\infty} \sum_{\xi=1}^{\infty} \frac{J_n(k_{qn}\rho_o^{'})J_n(k_{\xi n}\rho_s^{'})}{N_{\xi n}^2(k^2-k_{\xi n}^2)} \cos n(\phi_o^{'}-\phi_s^{'}) \tag{A4a}$$

where

$$N_{\xi n} = \left\{ \frac{\pi c^2}{\gamma_n} J_{n+1}^2(k_{\xi n}c) \right\}^{1/2} \tag{A4b}$$

$$\gamma_n = \begin{cases} 1 \;, & m=0 \\ \\ 2 \;, & m \neq 0 \end{cases}$$

In accordance with the procedure outlined in preceding paragraphs, let it be assumed that the combination of cylindrical waves, given by $\psi_{\nu m}$, is incident upon the inner conductor. The conductor is centered at the origin of the coordinate system (ρ,ϕ), shown in Fig. A1. The addition theorem for Bessel functions [15] is used to transform $\psi_{\nu m}$ (Eq.

(A2)) from the (ρ',ϕ') into the (ρ,ϕ) coordinate system. The resulting expression is given by

$$\psi_{\nu m}(\rho,\phi) = \sum_{p=0}^{\infty} E(m,p,e)J_p(k_{\nu m}\rho)\cos(p\phi) \tag{A5a}$$

where

$$E(m,p,e) = \frac{\gamma_p}{2}\left[J_{m-p}(k_{\nu m}e) + (-1)^p J_{m+p}(k_{\nu m}e)\right] \tag{A5b}$$

The scattered field can be expressed as a sum of outgoing cylindrical waves[2]

$$\psi^s = \sum_{p=0}^{\infty} A_p H_p^{(2)}(k_{\nu m}\rho)\cos(p\phi) \tag{A6}$$

where $H_p^{(r)}$ is the Hankel function of the second kind of order p. The unknown coefficients A_p are found by enforcing the boundary condition requiring $\Psi_{\nu m} = \psi_{\nu m} + \psi^s$ to vanish on $C_1(\rho=a)$. The incident-plus-scattered wave solution and its normal derivative evaluated on C_1 are given by

$$\Psi_{\nu m}(\rho,\phi) = \sum_{p=0}^{\infty} E(m,p,e)\left[J_p(k_{\nu m}\rho) - \frac{J_p(k_{\nu m}a)}{H_p^{(2)}(k_{\nu m}a)}\cdot H_p^{(2)}(k_{\nu m}\rho)\right]\cdot\cos(p\phi) \tag{A7}$$

$$\frac{\partial\Psi_{\nu m}}{\partial n}\Big|_{C_1} = -\frac{\partial\Psi_{\nu m}(\rho,\phi)}{\partial\rho}\Big|_{\rho=a} = -\frac{2j}{\pi a}\sum_{p=0}^{\infty} E(m,p,e)\frac{1}{H_p^{(2)}(k_{\nu m}a)}\cdot\cos(p\phi) \tag{A8}$$

where the Wronskian of Bessel's equation was used in deriving Eq. (A8). In the limit, as the radius a goes to zero, Eq. (A8) can be approximated by the following expression

$$\frac{\partial\Psi_{\nu m}}{\partial n}\Big|_{C_1} \approx \frac{2}{\pi a}\frac{E(m,0,e)}{f(k_{\nu m}a)} = \frac{2}{\pi a}\frac{J_m(k_{\nu m}e)}{f(k_{\nu m}a)} \tag{A9a}$$

where $f(k_{\nu m}a)$ is the small argument expansion of $jH_0^{(2)}$, given by [15]

2. $e^{j\omega t}$ time dependence is assumed throughout the thesis.

$$f(k_{\nu m}a) = \frac{2}{\pi} \left| \log\left(\frac{k_{\nu m}a}{2}\right) + \gamma \right| \tag{A9b}$$

and $\gamma = 0.5772$ is Euler's constant.

At this point, Eqs. (A4,A9) can be substituted into Eq. (A3) and the prescribed integration performed. The most expedient way to perform the integration is by transforming all the functions involving the variables of integration into the (ρ,ϕ) coordinate system. In the case of the Green function $G(\rho_0',\phi_0'|\rho_s',\phi_s')$, the required transformation is facilitated by the use of the addition theorem for Bessel functions. The transformation is applied to source coordinate (ρ_s',ϕ_s') and yields the following expression

$$G(\rho_0',\phi_0'|\rho_s',\phi_s')|_{C_1} = G(\rho',\phi'|\rho,\phi)|_{\rho=a} = \sum_{n=0}^{\infty} \sum_{\xi=1}^{\infty} \frac{J_n(k_{\xi n}\rho')}{N_{\xi n}^2(k^2-k_{\xi n}^2)} \cdot$$

$$\cdot \sum_{q=0}^{\infty} E(n,q,e) \, J_q(k_{\xi n}a) \, [\cos(n\phi') \cos(q\phi) + \sin(n\phi')\sin(q\phi)] \tag{A10}$$

where the subscript "0" is unambiguously omitted from ρ',ϕ'. Equation (A3) can now be rewritten as

$$\Psi_{\nu m}(\rho',\phi') \approx -\int_0^{2\pi} \left\{ -\frac{\partial \Psi_{\nu m}}{\partial \rho} \cdot G(\rho',\phi'|\rho,\phi) \right\}\bigg|_{\rho=a} \cdot (ad\phi), \tag{A11}$$

straightforward evaluation of which yields

$$\Psi_{\nu m}(\rho',\phi') = -\frac{4J_m(k_{\nu m}e)}{f(k_{\nu m}a)} \cdot \sum_{n=0}^{\infty} \sum_{\xi=1}^{\infty} \frac{J_n(k_{\xi n}e)J_n(k_{\xi n}\rho')}{N_{\xi n}^2(k^2-k_{\xi n}^2)} \cdot J_0(k_{\xi n}a)\cos(n\phi') \tag{A12}$$

As it stands, Eq. (A12) is not correct unless the parameter k is replaced by the modified cutoff wavenumber $K_{\nu m}$. Noting the fact that $\psi_{\nu m}$ and $\Psi_{\nu m}$ satisfy the wave equation, with wavenumbers $k_{\nu m}$ and $K_{\nu m}$, respectively, and using Green's theorem, it can

be shown that $K_{\nu m}$ satisfies the following formula [16]

$$K_{\nu m}^2 = k_{\nu m}^2 - \frac{\oint_{C_1} \psi_{\nu m} \frac{\partial \Psi_{\nu m}}{\partial n} dc}{\iint_{S_A} \psi_{\nu m} \Psi_{\nu m} ds}$$

(A13)

where S_A is the annular region bounded by C_O and C_I. Using the hypothesis that $\Psi_{\nu m}$ does not significantly differ from $\psi_{\nu m}$ over most of S_A, the integral in the denominator of Eq. (A13) can be approximated in the following manner

$$\iint_{S_A} \psi_{\nu m} \Psi_{\nu m} ds \approx \iint_{S_c} \psi_{\nu m}^2 ds = N_{\nu m}^2$$

(A14)

where S_C is the circular area bounded by C_O, and $N_{\nu m}$ is given by Eq. (A4b). Substitution of Eqs. (A5a) and (A9) into Eq. (A13) yields the following result

$$K_{\nu m}^2 \approx k_{\nu m}^2 - \frac{4 J_m^2(k_{\nu m}e) J_0(k_{\nu m}a)}{N_{\nu m}^2 f(k_{\nu m}a)}$$

(A15)

Note, the first term in the above expression for $K_{\nu m}^2$ is just the square of the original cutoff wavenumber, whereas the second term constitutes a small perturbation thereof.

To complete the derivation of $\Psi_{\nu m}$, a substitution of $K_{\nu m}$ for k in Eq. (A12) is made, and the result simplified using the fact that

$$K_{\nu m}^2 - k_{\xi n}^2 \approx \begin{cases} k_{\nu m}^2 - k_{\xi n}^2 & , \; \xi n \neq \nu m \\[2em] -\dfrac{4 J_m^2(K_{\nu m}e) J_0(k_{\nu m}a)}{N_{\nu m}^2 f(k_{\nu m}a)} & , \; \xi n = \nu m \end{cases}$$

(A16)

the final expression for $\Psi_{\nu m}$ can be written as follows

$$\Psi_{\nu m}(\rho', \phi') \approx \psi_{\nu m}(\rho', \phi') - \frac{4 J_m(k_{\nu m}e)}{f(k_{\nu m}a)} \times$$

$$\times \sum_{\substack{n=0 \\ \xi n \neq \nu m}}^{\infty} \sum_{\xi=1}^{\infty} \frac{J_n(k_{\xi n}e)J_n(k_{\xi n}\rho')}{N_{\xi n}^2 (k_{\nu m}^2 - k_{\xi n}^2)} \cdot J_0(k_{\xi n}a) \cos(n\phi') \tag{A17}$$

where in addition to the original wavefunction $\psi_{\nu m}$ there is a small term representing the perturbation by the inner conductor.

To verify the accuracy of the presented solution, a comparison is made between the results computed from Eq. (A15) and those obtained by the more rigorous technique of reference [11]. Lowest eight cutoff wavenumbers are plotted in Figs. A2, A3, as functions of the eccentricity e/c, for a/c ratios .01 and .03, respectively. The solid curves represent the data computed from Eq. (A15) and the markers are placed at points computed by the alternate method [11]. The agreement between the separately computed sets of data appears to be very good for the cases considered.

Clearly, the pertubation procedure outlined in this section is equaly applicable to the case where the outer boundary C_0 is a Perfect Magnetic Conductor (PMC). In fact the derivation of $K_{\nu m}$ and $\Psi_{\nu m}$ in that case is identical to the one presented above, and the results are formally given by Eqs. (A15) and (A17) with $N_{\nu m}$ replaced by

$$N_{\nu m} = \left\{ \frac{\pi c^2}{\gamma_m} \left[1 - \frac{m^2}{(k_{\nu m}c)^2} \right] J_m^2(k_{\nu m}c) \right\}^{1/2} \tag{A18}$$

Note, the results do not apply for the lowest cutoff wavenumber, which in the absence of the inner conductor is equal to zero. However, this does not present a major problem, since it can be readily computed by other methods.

Fig. A4 plots the modified cutoff wavenumbers for a waveguide with a PMC circular outer conductor and a PEC inner conductor. The ratio of the radii is $a/c = .022$. The solid curves are computed from Eq. (A15) with $N_{\nu m}$ given by Eq. (A18). The markers are
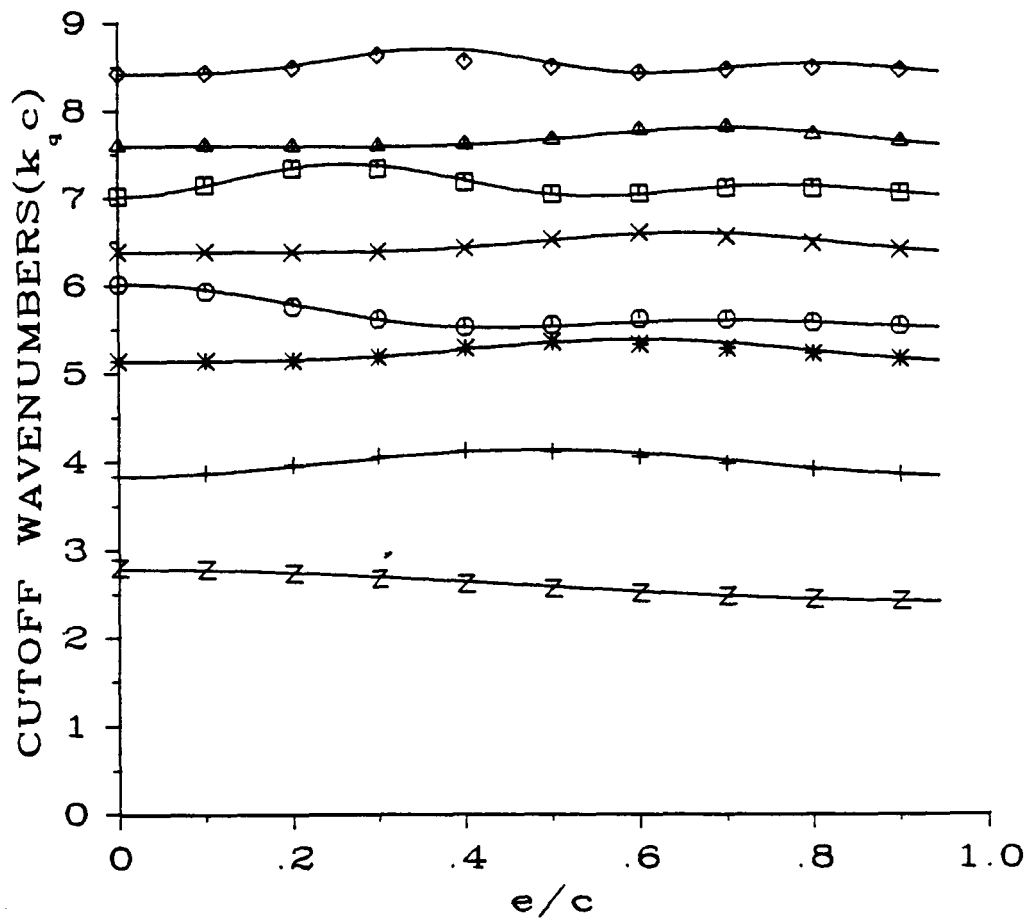
Figure A2. Cutoff wavenumbers for the TM modes in a waveguide with a PEC circular outer conductor and an eccentrically located PEC inner conductor, a/c = .01.
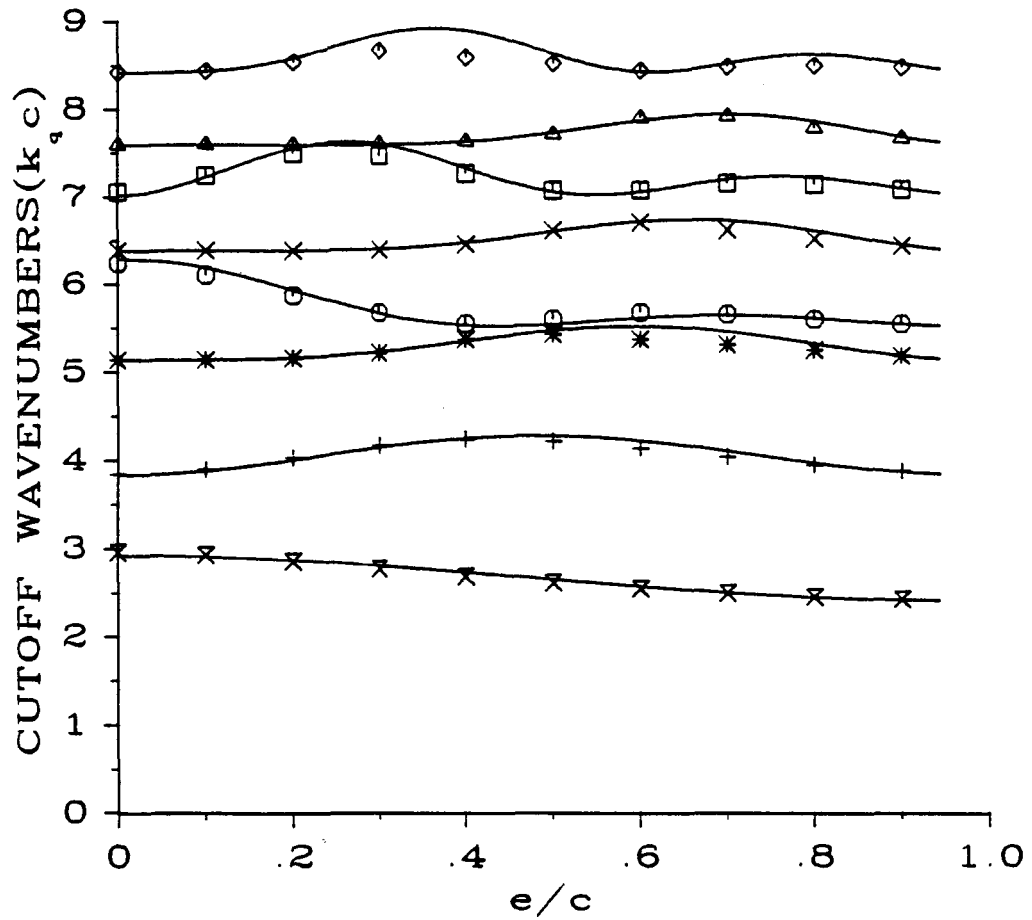
Figure A3.   Cutoff wavenumbers for the TM modes in a waveguide with a PEC circular outer conductor and an eccentrically located PEC inner conductor, a/c = .03.
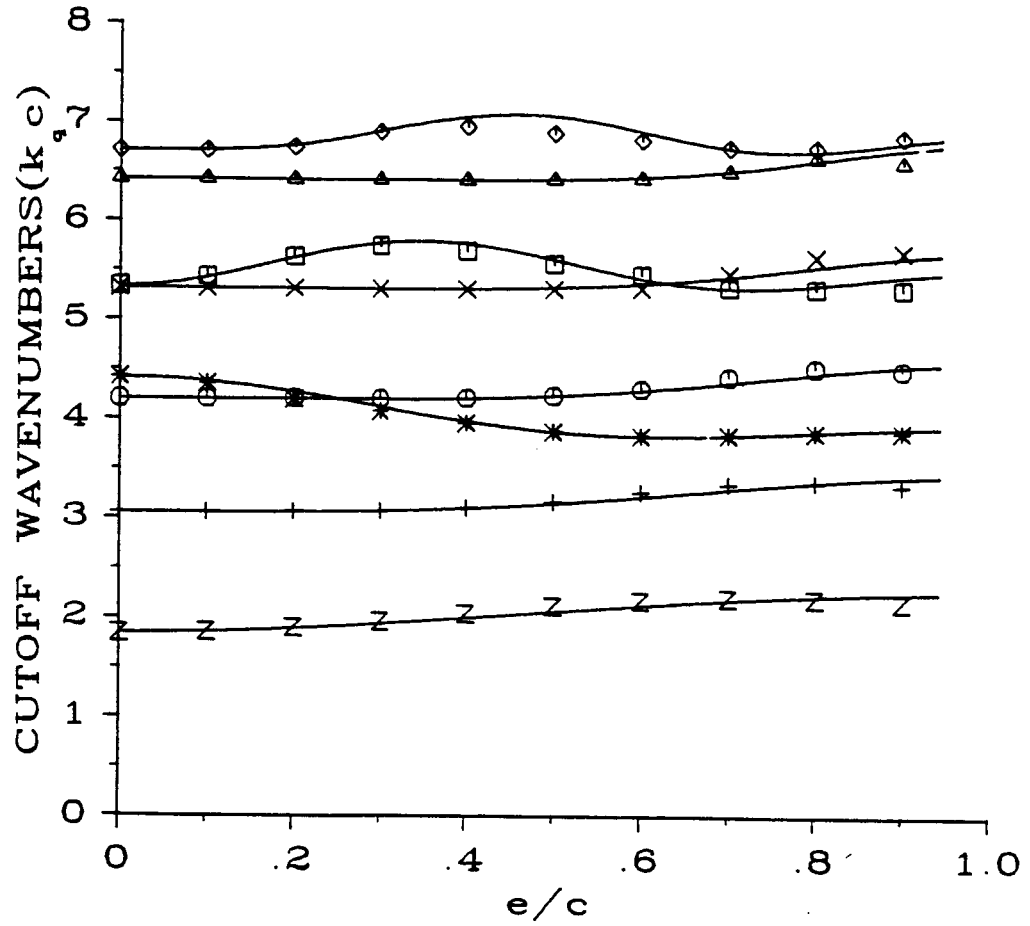
Figure A4. Cutoff wavenumbers for the TM modes in a waveguide with a PMC circular outer conductor and an eccentrically located PEC inner conductor, a/c = .022.

placed at data points obtained by the method outlined in Section 2.I.

A.III. Rectangular Waveguide with a Cylindrical Inner Conductor of Small Radius

Analysis of the circular waveguide with an eccentrically located inner conduction of small radius was presented in the preceding section. It should be noted, however, that the general technique used in Section A.II to derive the cutoff wavenumbers and the corresponding modes is applicable to other waveguide cross-section geometries. In this section it will be used to solve for the TM modes in a rectangular waveguide with inner conductor of small radius. Figure A5 illustrates the geometry, along with the relevant coordinate systems and dimensions. To avoid repetition and keep the presentation as brief as possible, all the assumptions and hypothesis stated in the preceding section will be omitted here. Only the most essential steps in the derivation will be shown, since it is completely analogous to the one found in Section A.II.

In the absence of the inner conductor, the "mn"th TM mode in a waveguide with a rectangular PEC outer boundary can be determined from the scalar potential function:

$$\psi_{mn} = \sin(k_{xm}x')\sin(k_{yn}y'); \tag{A19}$$

where

$$k_{xm} = \left(\frac{m\pi}{c}\right), \quad k_{yn} = \left(\frac{n\pi}{b}\right)$$

The wavefunction ψ_{mn} is expressible as a combination of four plane waves. It is assumed that these waves are incident upon the inner conductor. The scattering problem of plane wave by a circular cylinder is well documented [16] and its solution need not be reconsidered here. The total incident-plus-scattered wave $\Psi_{mn} = \psi_{mn} + \psi^s$, satisfying the homogeneous Dirichlet boundary condition on C_I, is found by superposition of the
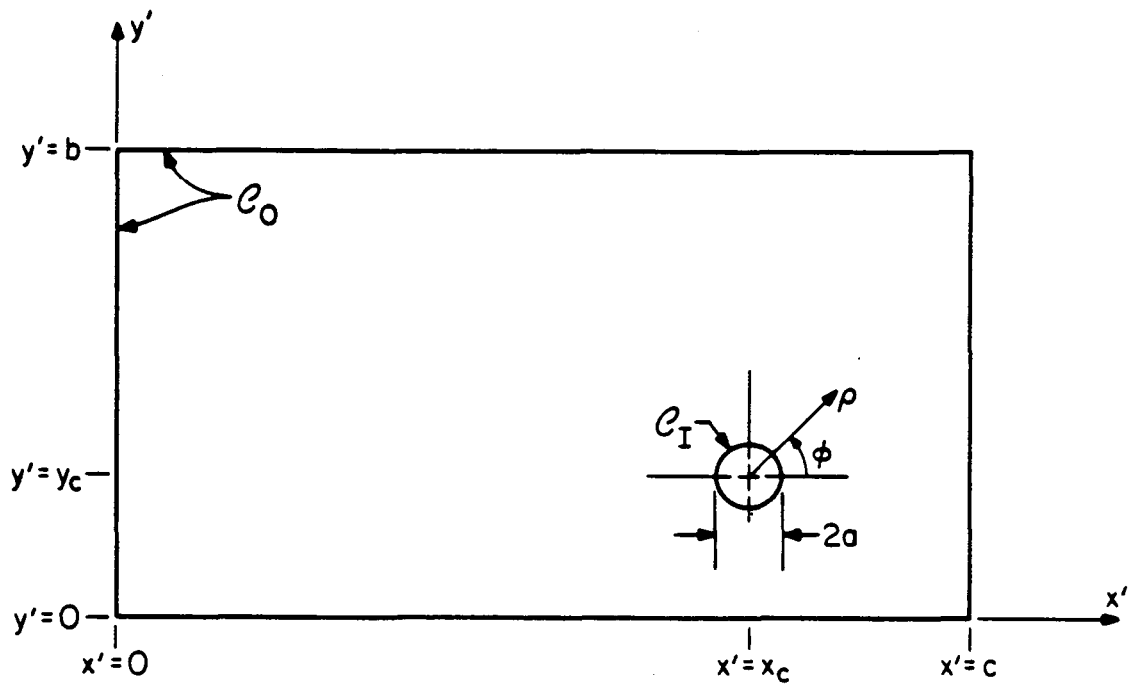
Figure A5. Cross-section of an annular waveguide with rectangular outer conductor.

solutions for the four plane waves constituting ψ_{mn}. As in Section A.II, the quantity of interest is the value of $\frac{\partial \Psi_{mn}}{\partial n}|_{C_1}$. Straightforward analysis shows that for small values of $k_{mn}a$

$$\frac{\partial \Psi_{mn}}{\partial n}|_{C_1} \approx \frac{2}{\pi a} \cdot \frac{\sin(k_{xm}x_c)\sin(k_{yn}y_c)}{f(k_{\nu m}a)} \qquad (A20)$$

where $k_{mn} = \sqrt{k_{xm}^2 + k_{yn}^2}$ and a , x_c, and y_c are as shown in Fig. 5.

The form of the modified wavefunction Ψ_{mn} at arbitrary points within the guide cross-section is found with the aid of Eq. (A3). For the case of rectangular waveguide being considered here, the Green function appearing in Eq. (A3) is given by

$$G(x_0',y_0'|x_s',y_s') = \sum_{p=1}^{\infty} \sum_{q=1}^{\infty} \frac{\sin(k_{xp}x_0')\sin(k_{yq}y_0')\sin(k_{xp}x_s')\sin(k_{yq}y_s')}{N^2 \ (k^2 - k_{pq}^2)} \qquad (A21a)$$

where

$$N = \frac{\sqrt{bc}}{2} \qquad (A21b)$$

Integration prescribed in Eq. (A3) is facilitated by several transformations of Eq. (A21). The source coordinates transformation $x_s' = x_c + \rho\cos\phi$, $y_s' = y_c + \rho\sin\phi$ is implemented first. This allows the term $\sin(k_{xp}x_s')\sin(k_{yq}y_s')$ in (A21a) to be rewritten as follows

$$\sin(k_{xp}x_s')\sin(k_{yp}y_s') = [\sin(k_{xp}x_c)\cos(k_{xp}\rho\cos\phi) + \cos(k_{xp}x_c)\sin(k_{xp}\rho\cos\phi)] \times$$

$$\times [\sin(k_{yq}y_c)\cos(k_{yq}\rho\sin\phi) + \cos(k_{yq}y_c)\sin(k_{yq}\rho\sin\phi)] \qquad (A22)$$

Equation (A22) is further expanded in a series of terms involving Bessel functions $J_\nu(k_{xp}\rho)$, $J_\nu(k_{yq}\rho)$ and angular harmonics $\cos(\nu\phi)$, $\sin(\nu\phi)$ [15]. The first and only term of

the expansion required for subsequent calculations is given by

$$\sin(k_{xp}x_s')\sin(k_{yq}y_s') \approx \sin(k_{xp}x_c)\sin(k_{yq}y_c)J_0(k_{xp}\rho)J_0(k_{yq}\rho) \qquad (A23)$$

Substitution of Eqs. (A20) and (A21a) into Eq. (A3) and subsequent use of Eq. (A23), yields the formal expression for the modified wavefunction Ψ_{mn}:

$$\Psi_{mn}(x',y') \approx \frac{-4\,\sin(k_{xm}x_c)\sin(k_{yn}y_c)}{f(k_{mn}a)} \cdot \sum_{p=1}^{\infty}\sum_{q=1}^{\infty} \frac{\sin(k_{xp}x')\sin(k_{yq}y')\sin(k_{xp}x_c)}{N^2\,(k^2-k_{pq}^2)} \cdot$$

$$\cdot \sin(k_{yq}y_c) \cdot J_0(k_{xp}a)J_0(k_{yq}a) \qquad (A24)$$

As previously noted in Section A.II, Eq. (A24) is not correct until and unless k is replaced by the modified wavenumber K_{mn}. Equation (A13) is used to calculate K_{mn}, which after some analysis can be shown to satisfy the following formula

$$K_{mn}^2 \approx k_{mn}^2 - \frac{4\,\sin^2(k_{xm}x_c)\sin^2(k_{yn}y_c)}{N^2\,f(k_{mn}a)} \cdot J_0(k_{xm}a)J_0(k_{yn}a) \qquad (A25)$$

The final form of the modified wavefunction Ψ_{mn} is obtained when Eq. (A25) is substituted into Eq. (A24) and the resulting expression simplified in the manner previously described in Eq. (A16):

$$\Psi_{mn}(x',y') \approx \psi_{mn}(x',y') - \frac{4\,\sin(k_{xm}x_c)\sin(k_{yn}y_c)}{f(k_{mn}a)} \cdot$$

$$\cdot \sum_{\substack{p=1 \\ pq \neq mn}}^{\infty}\sum_{q=1}^{\infty} \frac{\sin(k_{xp}x')\sin(k_{yq}y')\sin(k_{xp}x_c)\sin(k_{yq}y_c)}{N^2(k_{mn}^2-k_{pq}^2)} \cdot J_0(k_{xp}a) \cdot J_0(k_{yq}a) \qquad (A26)$$

Figures A6(a,b) plot the variation of K_{mn} with x_c, for a rectangular waveguide with ratio b/c = 0.5. The results are plotted over the domain $0.5 \leqslant x_c/c \leqslant .97$, $y_c/c = 0.1, 0.2$.
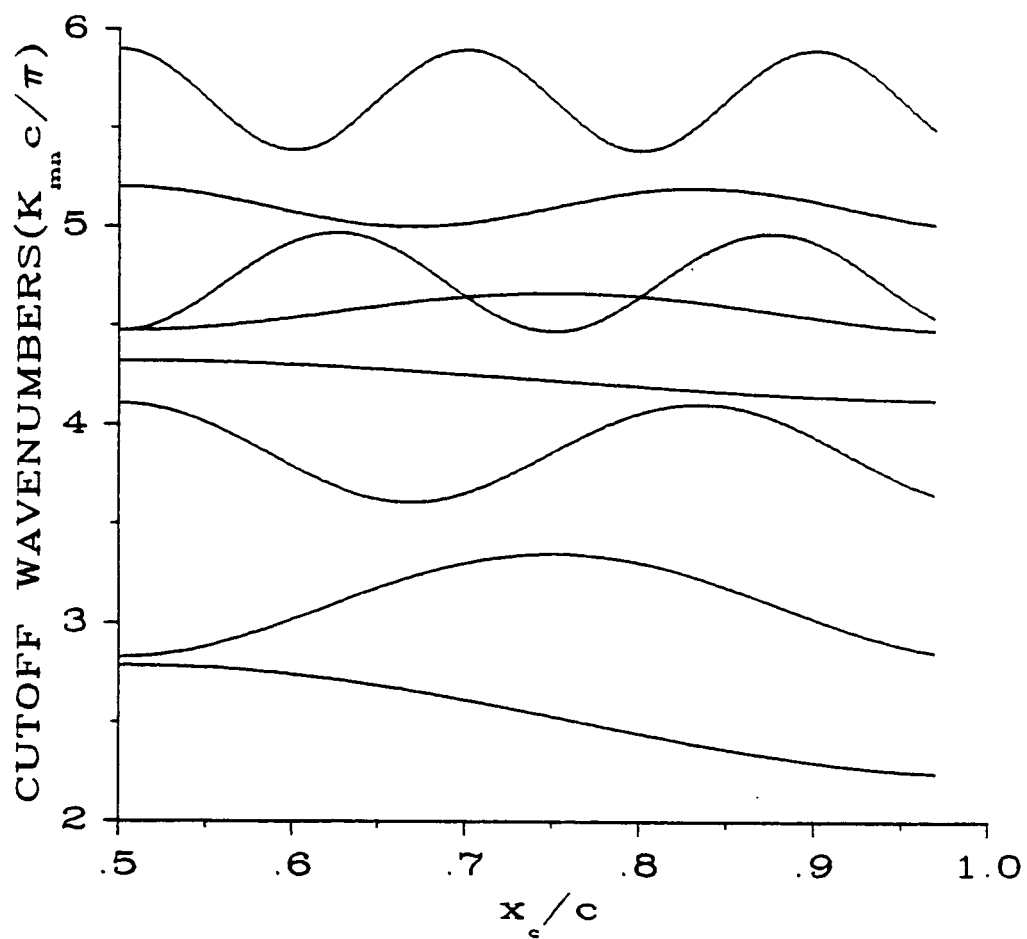
Figure A6(a). Cutoff wavenumbers for the TM modes in a waveguide with a PEC rectangular outer conductor and an eccentrically located PEC inner conductor, $b/c = 0.5$, $a/c = 0.03$, $y_c/c = 0.1$.
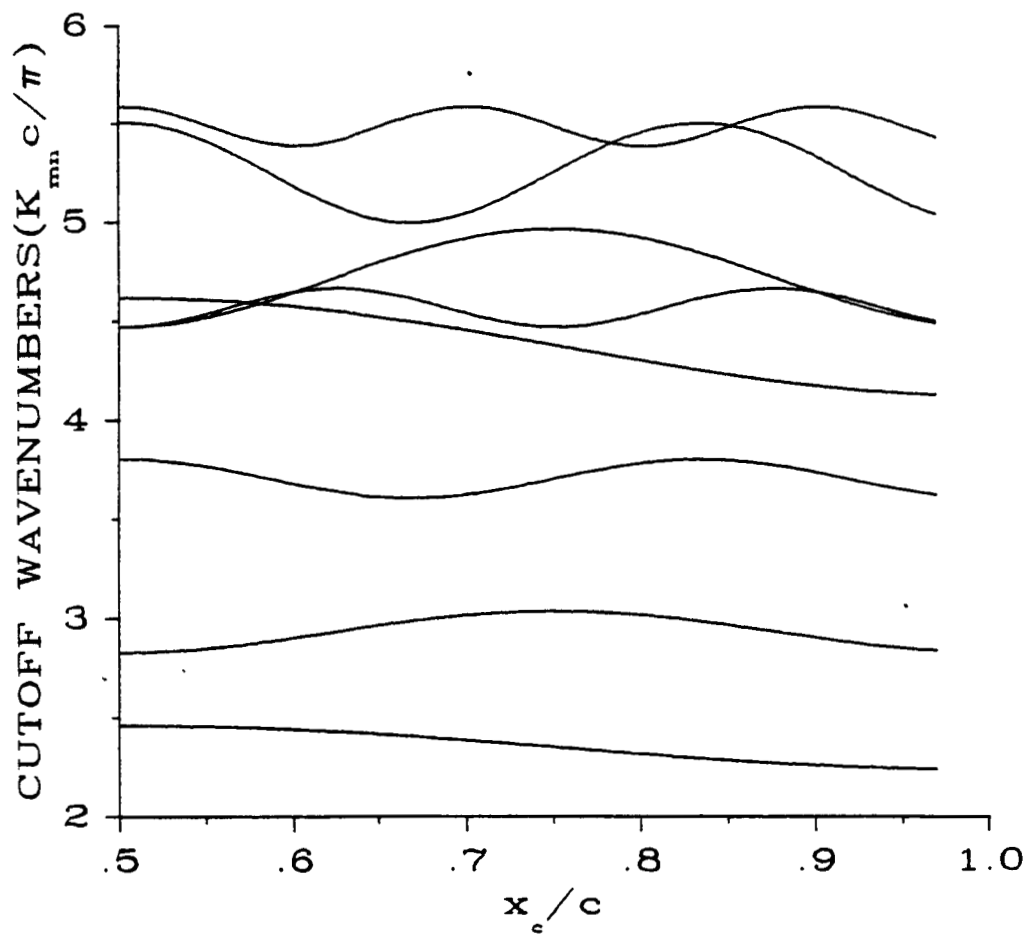
Figure A6(b).   Cutoff wavenumbers for the TM modes in a waveguide with a PEC rectangular outer conductor and an eccentrically located PEC inner conductor, $b/c = 0.5$, $a/c = 0.03$, $y_c/c = 0.2$.